AD-A051 987 AVCO EVERETT RESEARCH LAB INC EVERETT MASS F/G 20/9
ELECTRON-BEAM SUSTAINER DISCHARGE STREAMERS AND ARCING.(U)
NOV 77 D H DOUGLAS-HAMILTON, P S ROSTLER F44620-75-C-0025
AFOSR-TR-78-0354 NL

UNCLASSIFIED

| OF |
AD
A051 987

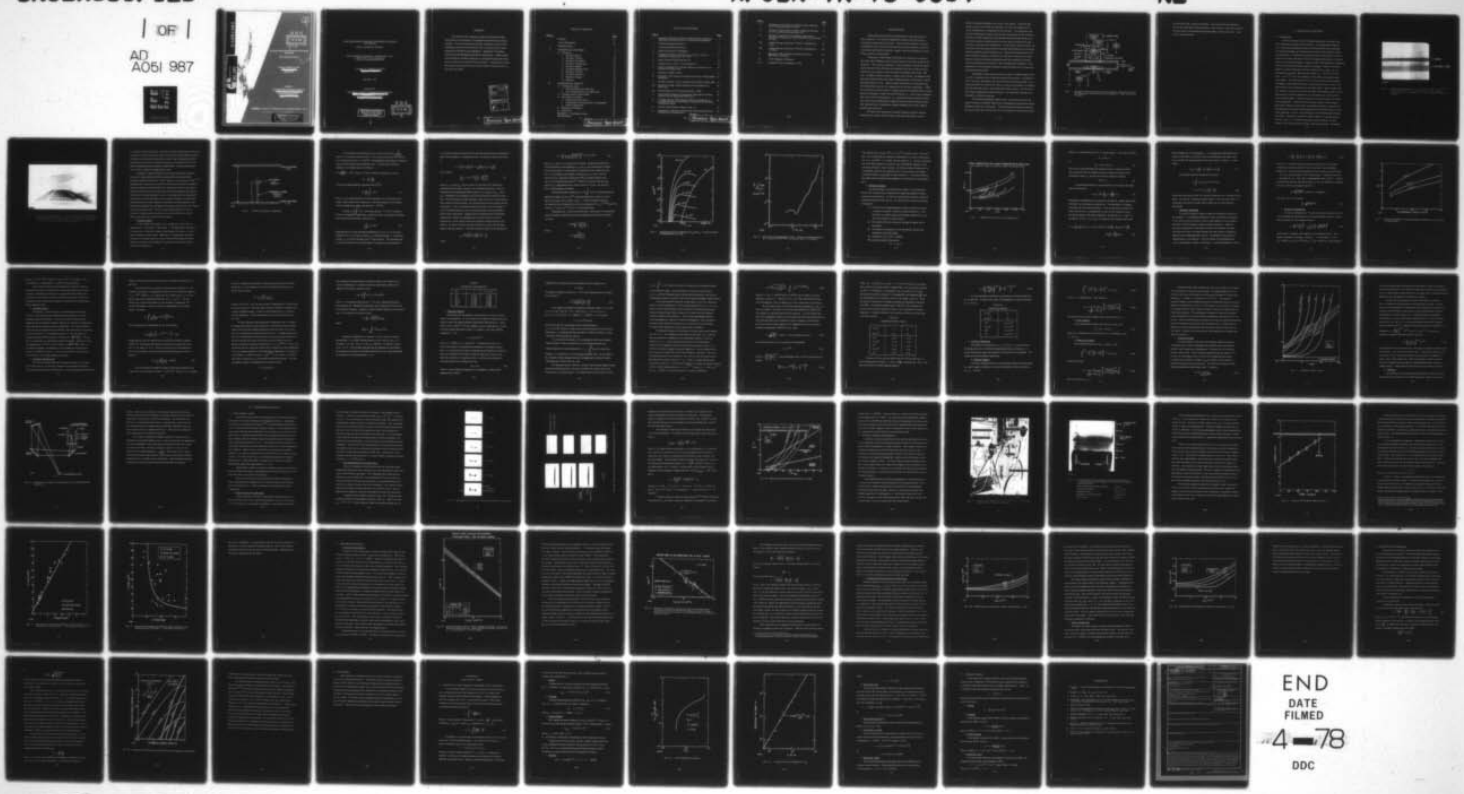

END
DATE
FILMED
4-78
DDC

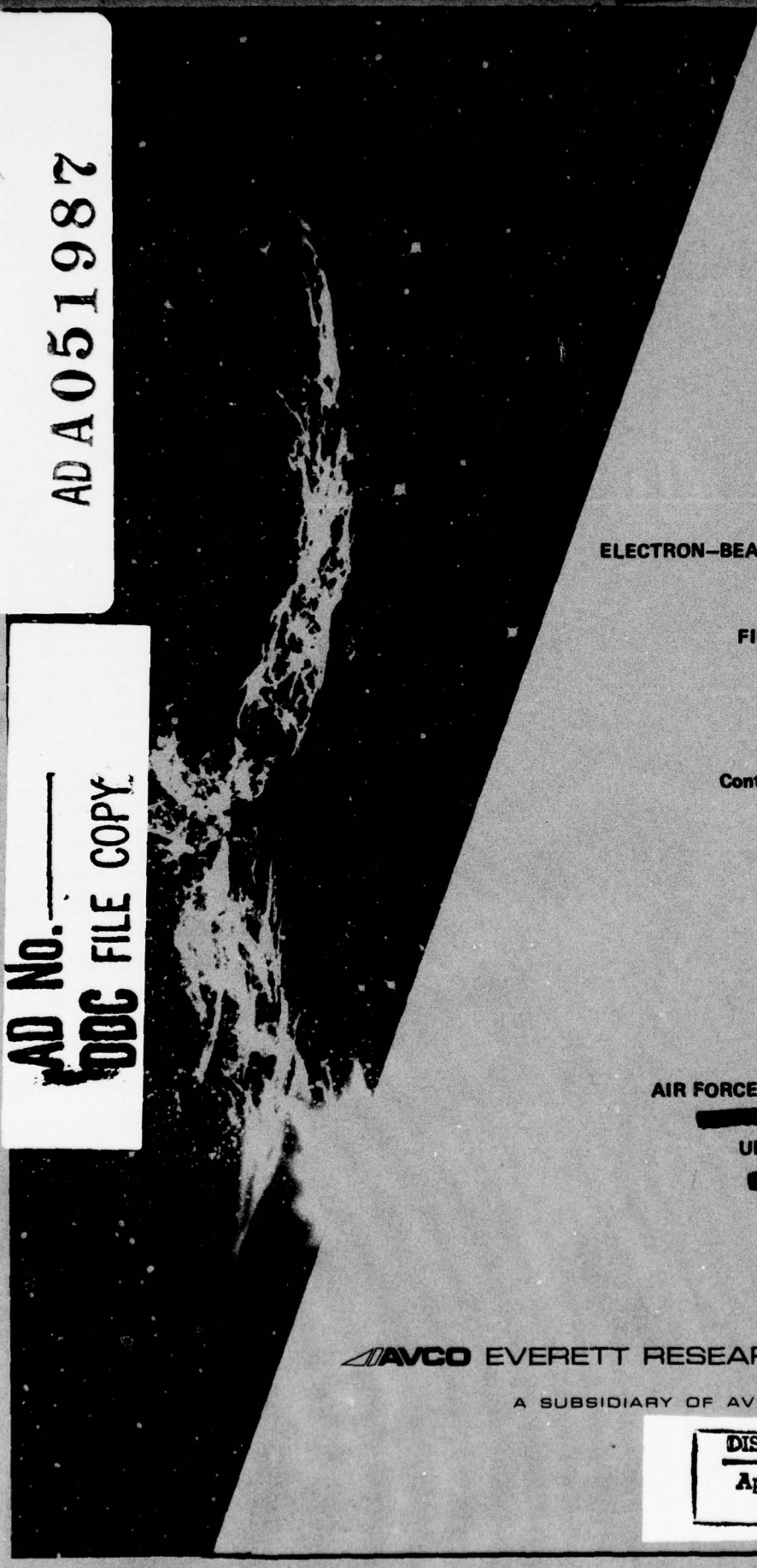

ELECTRON-BEAM SUSTAINER DISCHARGE STREAMERS AND ARCING

FINAL TECHNICAL REPORT

Contract No. F44620-75-C-0025

[redacted]

November 1977

prepared for

AIR FORCE OFFICE OF SCIENTIFIC RESEARCH

[redacted]

UNITED STATES AIR FORCE

[redacted]

AVCO EVERETT RESEARCH LABORATORY, INC.

A SUBSIDIARY OF AVCO CORPORATION

ELECTRON-BEAM SUSTAINER DISCHARGE STREAMERS AND ARCING

FINAL TECHNICAL REPORT

AVCO EVERETT RESEARCH LABORATORY, INC.
a Subsidiary of Avco Corporation
Everett, Massachusetts 02149

Contract No. F44620-75-C-0025
[redacted]

November 1977

prepared for

AIR FORCE OFFICE OF SCIENTIFIC RESEARCH
[redacted]
UNITED STATES AIR FORCE
[redacted]

ABSTRACT

The electron beam sustainer method of generating a stable high pressure gas discharge is investigated theoretically and experimentally. The most important discharge instability in the non-self-sustaining discharge is the streamer; this is discussed and a model proposed for formation and propagation. Integration of streamer velocity over the discharge gap predicts arcing times. Experimental measurements of streamer behaviour in nitrogen discharge have been made, and these are compared with predictions. Comparisons in other gas mixtures and various electron-beam sustainer discharge devices have also been made.

TABLE OF CONTENTS

LIST OF ILLUSTRATIONS

I. INTRODUCTION

Stable high-density plasma discharges have many applications in plasma physics. An especially significant example is the use of these discharges in high-power gas lasers. The work described here concerns investigation of the external ionization electron-beam sustainer method of producing a high-density discharge, together with the advantages and instabilities peculiar to that system.

Classically, stable plasma discharges are produced by working in the region where diffusion of the charged species to the walls stabilizes the discharge. The electron temperature in the discharge is raised (by adjusting the electric field, E/P) until the ionization rate due to these electrons equals the rate at which electron-ion pairs recombine at the walls. However, at higher pressures and/or in larger scale devices, the diffusion time generally becomes longer than other instability times in the plasma, and the discharge spokes or arcs. Many of these instabilities are associated with the ionization process and its coupling with the electron temperature. AERL has constructed a facility under a company-sponsored program which produces uniform discharges in which the electron density, n_e, can be varied independently of the electron temperature, T_e. Separation of the ionization process from the electron temperature is achieved in this facility by having a separate control on each, resulting in a stable discharge over a wide range of pressure and scale size.

We achieve the separation of plasma ionization from the electron temperature by using a beam of high-energy electrons (EB) to create a

uniform ionization throughout the volume of the plasma. Using the high energy electrons to provide the ionization, the electron temperature is varied independently by adjusting the electric field. It is found that if the electron temperature is kept so low that the ionization due to the discharge electrons is small compared to the ionization due to the high energy electrons the discharge remains uniform over the range of pressures investigated (up to and above one atmosphere). As the electric field is raised, the ionization by the discharge electrons becomes substantial and the discharge becomes nonuniform and eventually arcs. Stable discharge behavior is obtained when the volumetric electron loss rates due to electron-ion recombination and electron-neutral attachment equal the volumetric secondary electron production rate by the EB. The recombination coefficient α and attachment β are important parameters determining the level of ionization obtainable with given EB.

Discharges of this type are used by a number of ARPA-funded lasers in order to maximize laser output from high pressure gases. In addition to 10.6μ CO_2 laser discharges, the electron-beam sustainer principle is currently being used for CO and HF lasers, as well as the initiation of chemical fluorine-deuterium lasers, and xenon halide visible lasers. In view of the wide range of application of this discharge, it is especially valuable to investigate its stability properties.

The discharge apparatus shown in Fig. 1 has been used under the present contract to measure electron ion recombination and electron neutral attachment rates in various gases. The dissociative attachment instability discovered under this contract has led to investigation of discharge stability,

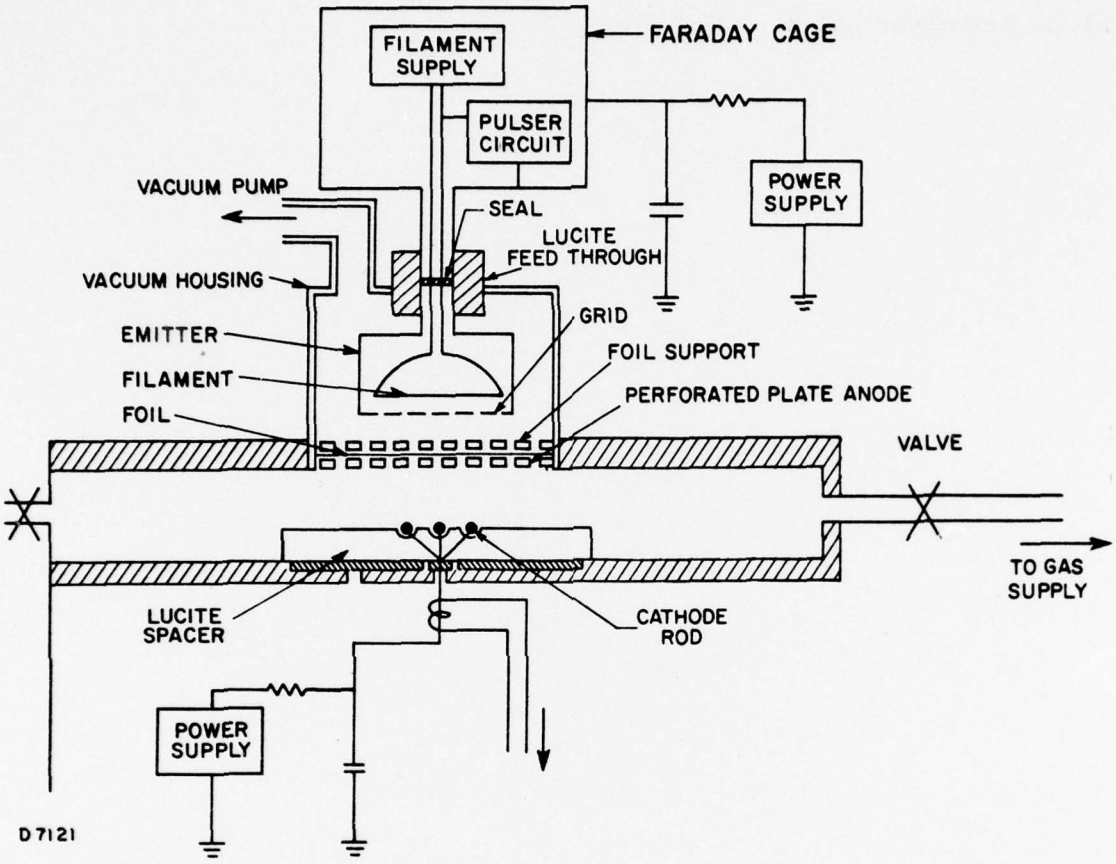

Fig. 1 Schematic Drawing of Electron-Beam Sustainer Discharge, Showing the Electrodes used for Streamer Investigations. Optic axis is into the paper.

or more precisely, modes of instability. The most prominent instability mode in the externally ionized discharge is the streamer, and some progress has been made in understanding this phenomenon in the present case. This will be discussed below.

II. THEORETICAL DISCUSSION

A. STREAMERS

The most obvious form of discharge instability occurring in non self-sustaining discharges is the streamer. This phenomenon appears as a visible glowing projection from one discharge electrode, generally the cathode (although anode streamers have been observed under certain circumstances). The projection moves across the discharge at a velocity near that of sound, and when it reaches the opposite side an arc is formed short-circuiting the discharge. Figures 2 and 3 show examples of streamers produced in an electron-beam sustainer discharge. Figure 2 is a photograph of a pulsed discharge in the gas mixture He: N_2: CO_2: 3: 2: 1 at atmospheric pressure. With electron density $n_e \sim 3 \times 10^{12}$ cm^{-3} and $E/N \sim 2 \times 10^{-16}$ V cm^2, the cathode is at the lower side and the anode at the upper. The electron beam used to ionize the non-self-sustaining discharge is introduced from below, and the electrons are of such a voltage that they do not densely ionize the anode region. Since current must be conserved, the electric field in this region rises sharply, and becomes high enough to cause the generation of anode streamers, visible at the top of the photograph. Cathode streamers are also visible at the bottom of the photograph. Usually the electron beam energy is high enough so that anode streamers hardly exist and cathode streamers, growing from discontinuities associated with the cathode and the cathode layer, are the most important. In Fig. 3 the streamers of a CW flowing gas discharge are shown. Gas flow is from left to right at Mach 0.4, the gas used is He: N_2: CO_2 16: 8: 1 at 380 torr pressure, and the cathode is at the bottom, from which the electron beam enters the discharge. Streamers

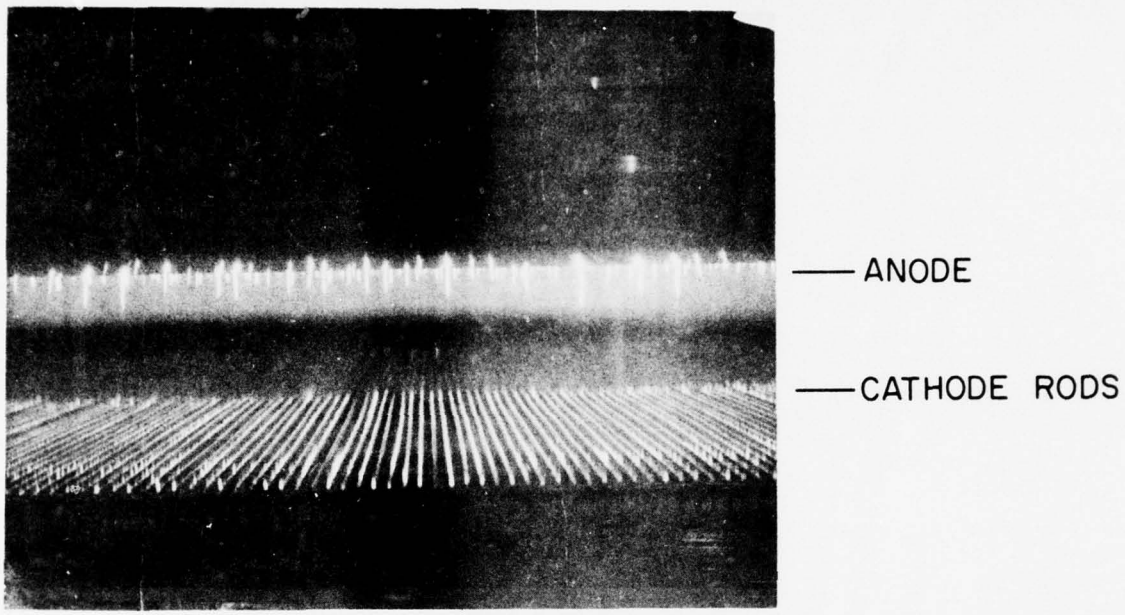

E1075

Fig. 2 Pulsed Discharge Streamers. Electron density ~ 3×10^{12} cm^{-3}, electric field 5000 V/cm, pressure 1 atm. Gas mixture He: N_2: CO_2; 3: 2: 1. Electron beam enters through cathode, at bottom.

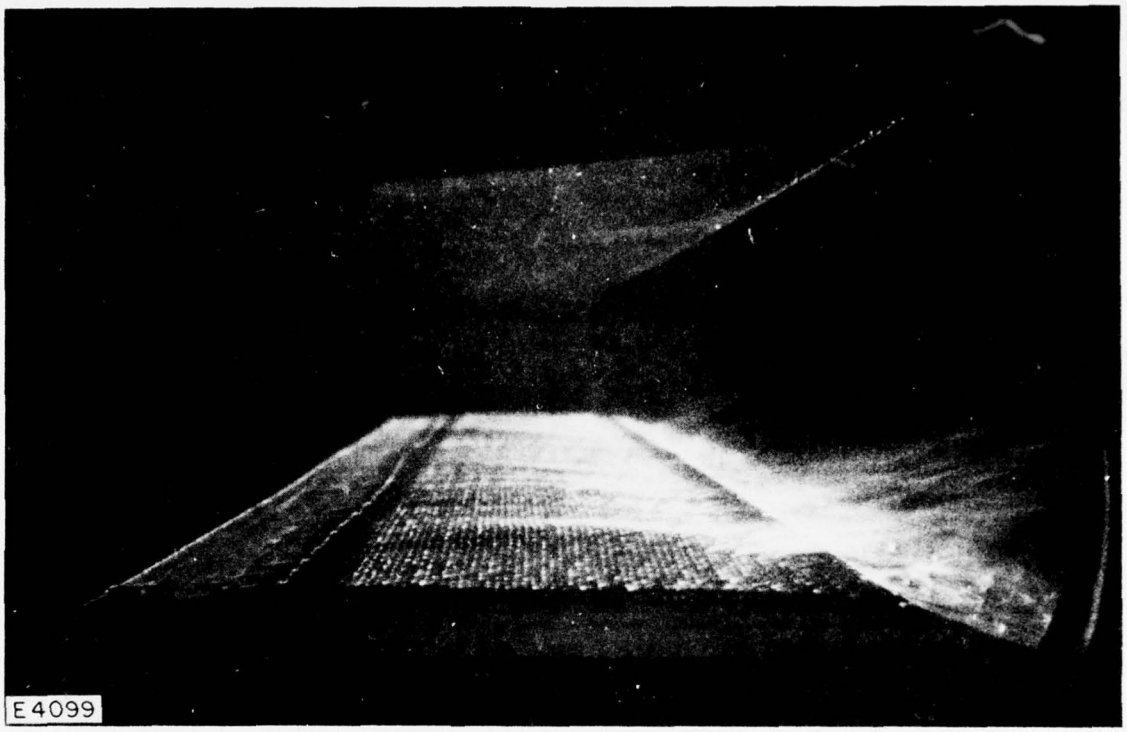

Fig. 3 Flowing Discharge Streamers. Flow is from left to right: electron beam enters through cathode, at bottom. Pressure 380 torr, flow velocity Mach 0.4, electron density 3×10^{11} cm^{-3}, electric field 2.8 kV/atm cm, gas mixture He: N_2: CO_2; 16: 8: 1.

are visible leaving the cathode: they then are blown downstream and become complicated. Anode streamers can also be seen leaving the upper electrode, and they are also blown downstream; arcing in such discharges generally takes place several cavity widths downstream, presumably when the displaced cathode and anode streamers finally meet. In the present discussion we will consider the simpler static case.

Attempts to explain streamers on the basis of electron reproduction rates in high-intensity fields have generally been unsuccessful, leading to predicted velocities ~ c/100, where c is the velocity of light.[1, 2] Although these velocities are correct for the initiation of spark breakdown electron avalanche in gases subjected to high electric fields, this type of avalanche cannot occur in the low fields of the nonselfsustaining discharge. The process forming streamers in such a discharge must be a gasdynamic heating effect in which gas near a discontinuity is heated to a sufficiently high temperature so that it becomes conductive; the discontinuity is then effectively propagated out through the discharge in the form of a hot, highly conducting column of gas. We will examine the properties of such a streamer, simplifying the discussion as much as possible in order to obtain analytical and avoid numerical solutions.

1. Streamer Model

We will regard the streamer as a cylindrical column of gas at temperature T, with radius b and length c. We approximate the head of the streamer as a sphere of highly conducting gas of radius a, in which joule heating of the gas occurs. (See Fig. 4) The pressure inside the streamer is assumed identical to that in the main discharge (if it were higher the streamer would expand in all directions near sonic velocity into the discharge gas).

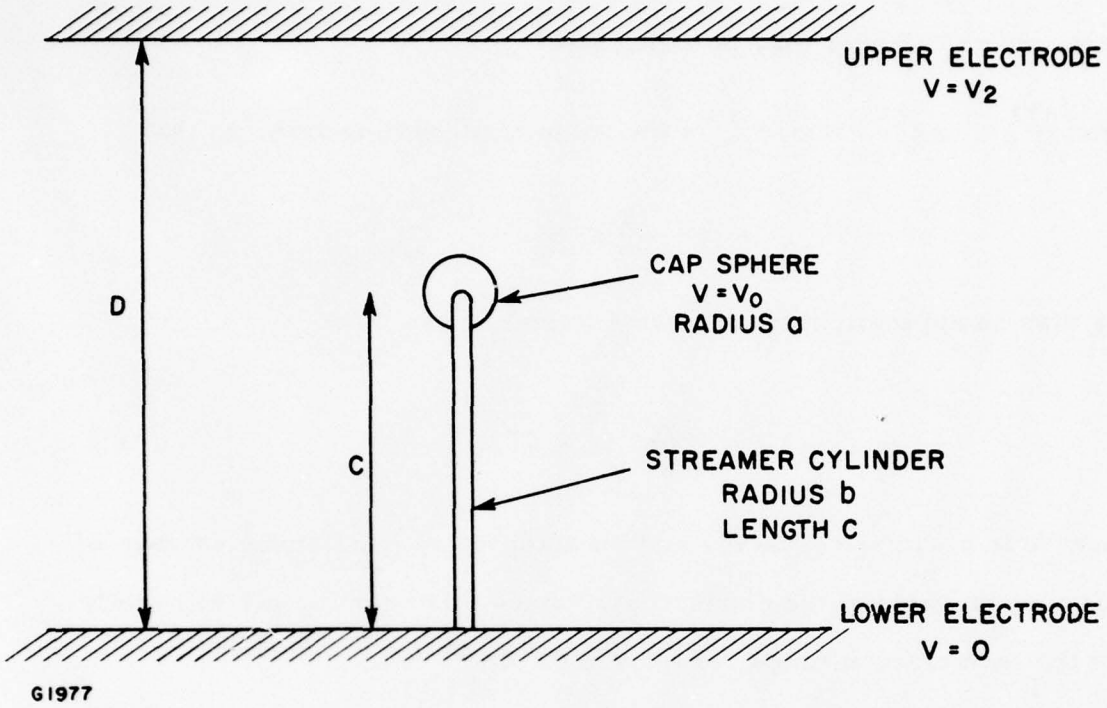

Fig. 4 Model for Streamer Propagation

The volumetric joule heating in the cylinder will then be $\frac{I^2}{(\pi b^2)^2 \sigma}$ where σ is the gas conductivity and I is the current carried in the cylinder. For temperatures below ~ 3×10^4 °K, in atmospheric pressure gas conductive heat loss will greatly exceed radiative loss. The thermal conduction equation for a cylinder may be written as

$2 \pi r \kappa \left(\frac{dT}{dr}\right) = - \pi r^2 \dot{q}$, where $\dot{q}$ is the volumetric heating rate, so that

$$\dot{q} = - \frac{2}{R} \kappa \frac{dT}{dR} .$$

This may be approximated, following Raizer,[3] as

$$\dot{q} = \frac{A}{R^2} \int_0^T \kappa \, dT, \qquad (1)$$

where A is a numerical factor and the integration is a convenient way of using a mean value of the conductivity, since this quantity varies greatly over the temperature range considered ($T < 10^4$ °K).

Writing $\bar{\kappa} = \frac{1}{T} \int_0^T \kappa \, dT$, and noting that for $T < 3 \times 10^4$ radiation losses are negligible compared to conduction losses, we equate the heating and cooling rates and obtain, placing R = b,

$$\frac{I^2}{\pi b^2 \sigma} = \pi A \bar{\kappa} T \qquad (2)$$

Adopting Raizer's value for high temperature air, A ≈ 15, we write the conductivity as $\sigma = n_e e \mu_o / N$, where n_e is electron density, e is electron charge, μ_o is electron mobility and N is gas density. We will determine n_e from the solution for the Saha equation in the gas at the temperature

T considered, and the density will be inversely proportional to temperature under the assumption of constant pressure, so that the conductivity scales as

$$\sigma = \sigma_o \left[(T/T_o) \left\{ n_e(T) + n_{eo} \right\} / \left\{ n_e(T_o) + n_{eo} \right\} \right]$$

and we obtain

$$\frac{I^2}{\pi b^2} = 15 \pi \kappa T^2 \frac{\sigma_o}{T_o} \left[1 + \frac{n_e(T)}{n_{eo}} \right] \qquad (3)$$

where σ_o, T_o and n_{eo} are the values for the electrical conductivity, temperature and electron density in the undisturbed medium, $n_e(T)$ is obtained from the appropriate Saha equation, and $n_e(T_o) \ll n_{eo}$. Here n_{eo} corresponds to the density of electrons produced by external ionization. The dissociation of molecular gas, which will occur at the temperatures attained in the streamer, will increase the electron mobility and the conductivity. In Eq. (3) we have ignored this effect since the change in $n_e(T)$ with temperature is much more rapid and has much the greater effect on the conductivity. Equation (3) now expresses the relationship between the current in a cylindrical gas column of radius b and its temperature, in the regime where the dominant cooling process is conductive. In order to use this we need the function $n_e(T)$ from the Saha equation and the current I. The first of these is given by the expression

$$n_e = \frac{L_o T_o P_o}{T} \frac{f}{2} \left[\sqrt{1 + \frac{4}{f}} - 1 \right] ,$$

where

$$f = 2 \frac{u_1}{u_o} \frac{1}{T_o L_o \beta} \left(\frac{2\pi m_e k}{h^2} \right)^{3/2} T^{5/2} e^{-I/kT} \qquad (4)$$

and L_o, T_o and P_o are Loschmidt's number, initial gas temperature (^oK) and pressure in atmospheres, u_1 and u_o are the statistical weights of the ion and atom, β is the degree of dissociation for a molecular gas ($\beta = 2$ for nitrogen in the regime of interest), m_e, k and h are the electron mass, Boltzman constant and Planck constant respectively, and I is the ionization potential.[4] Values of n_e derived for pure N_2, and for N_2 contaminated with a molar fraction ψ of Na, are shown in Fig. 5 at atmospheric pressure.

The mean thermal conductivity, $\bar{\kappa} = \frac{1}{T} \int_o^T \kappa \, dT$, is derived from the published conductivity for air[5] at high temperatures, which is close to that for nitrogen, and is shown in Fig. 6. Over the range of interest this quantity can be fitted fairly well by the expression $\bar{\kappa} = \kappa_o T^{1.893}$ w/cm/^oK, where $\kappa_o = 3.145 \times 10^{-10}$ and T is in degrees Kelvin.

Combining Eqs. (3) and (4) with the above expression for conductivity yields an implicit equation for the gas temperature at which the streamer can exist:

$$T^{3.893} \left(1 + \frac{n_e(T)}{n_{eo}} \right) = C \qquad (5)$$

where

$$C = \frac{I^2 T_o}{15\pi^2 b^2 \kappa_o \sigma_o}$$

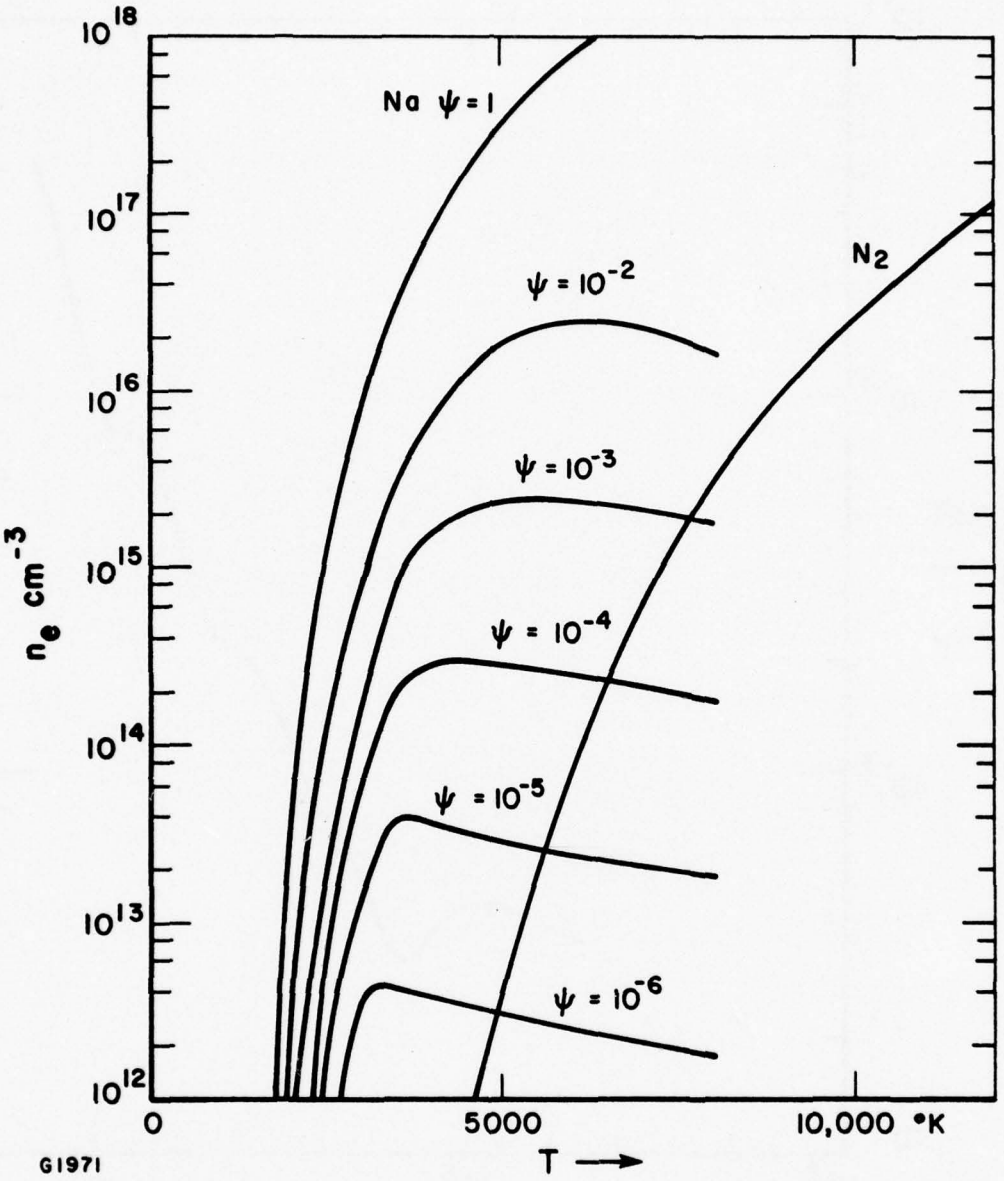

Fig. 5 Equilibrium Electron Density for N_2 and N_2 + ψ Na as Function of Temperature, at 1 atm

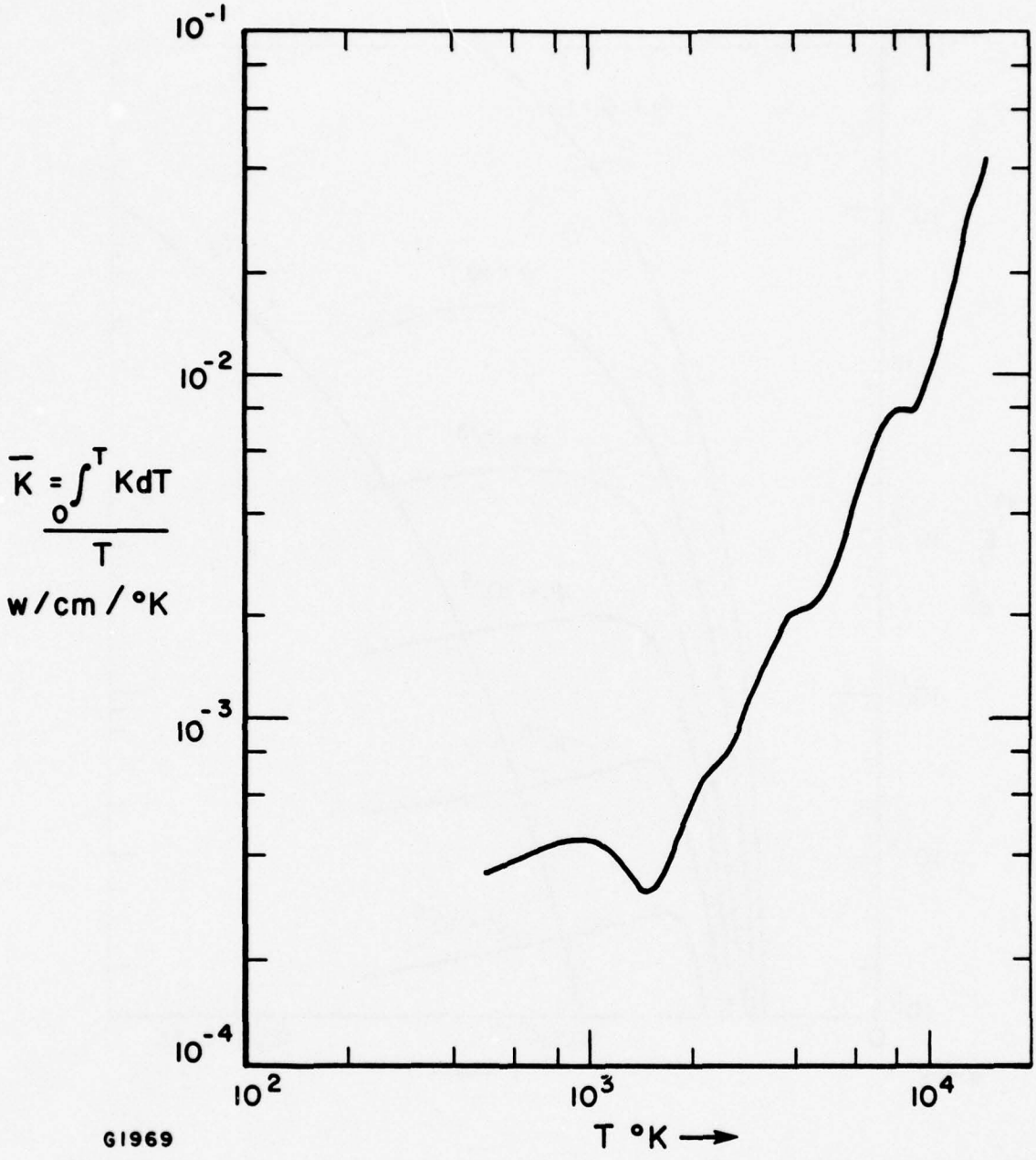

Fig. 6 Mean Thermal Conductivity for Air. This can be approximated as $\bar{K} = 3.145 \times 10^{-10} T^{1.893}$, T in °K for $1500 < T < 15,000$.

The solution of Eq. (5) for $10^{15} \leq C \leq 10^{20}$ is shown in Fig. 7 for nitrogen. It is evident that the streamer temperature is a slowly varying function of C, and $5000 < T < 10,000$ over this range of C. We note in passing that if the Saha equation is solved for gas containing an impurity of low ionization potential, such as sodium, the stable streamer temperature is considerably reduced, and solutions to Eq. (5) are shown for nitrogen with added sodium contaminant of molar fraction ψ. We might therefore anticipate faster formation and propagation of streamers in contaminated gas.

2. Streamer Current

The next problem is to estimate the current I in the streamer. Most of the current will be collected in the high-field spherical region at the tip of the streamer. In order to calculate this we need to know the potential distribution near the tip. We will therefore make the following assumptions:

(1) The field can be approximated by that of a sphere of radius a between two plates: denote the sphere potential V_1, the top plate V_2, bottom plate zero and plate separation D, distance from sphere to bottom plate c.

(2) All current enters the streamer through the upper half of the sphere.

(3) The sphere is attached by a thin conducting cylinder (the streamer) to the lower plate.

(4) The field is $E_o = V_2/D$ at infinity.

The continuity equation then gives

$$\nabla \cdot j = \dot{q} = 0$$

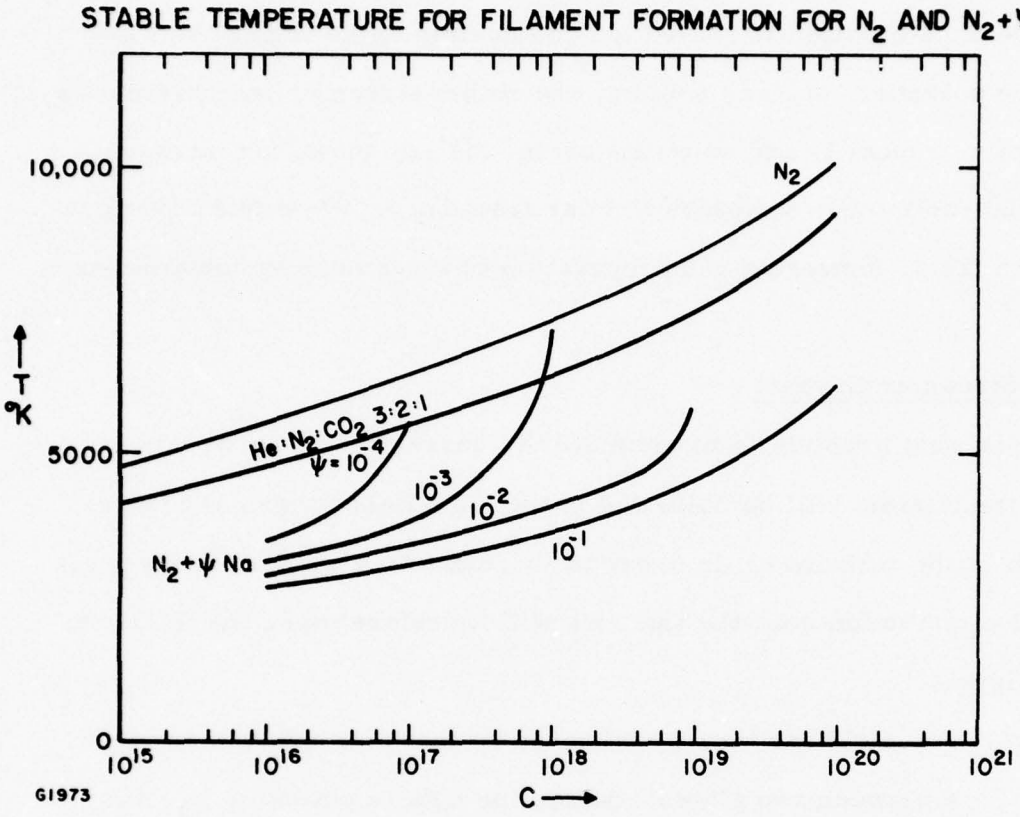

Fig. 7 Solution to Eq. (5) for T as Function of C

where j is current density and q is charge density. This may be written

$$\nabla \cdot (\sigma E) = 0$$

or

$$\nabla \sigma \cdot \nabla V + \sigma \nabla^2 V = 0 \tag{6}$$

Since we are approximating the streamer tip as a conducting sphere, the conductivity will be constant outside the sphere and equal to the undisturbed value σ_o, and Eq. (6) becomes Laplace's equation

$$\nabla^2 V = 0 \tag{7}$$

The potential field for a charged sphere in an infinite field must then be of the form:

$$V = a_1 + \frac{b_1}{r} + \left(a_2 r + \frac{b_2}{r^2}\right)\cos\theta, \tag{7a}$$

using polar coordinates (r, θ) centered on the sphere, higher terms being eliminated by the boundary condition (4). This expression is slightly erroneous near the electrode plates, where image effects increase the field, but the error is unimportant for most of the streamer motion between the plates, and will be neglected. Noting that $a_2 = -b_2/a^3$ on the sphere, and $V_1 = a_2 + b_2/a$, we eliminate the constants and obtain:

$$V = \frac{1}{1 - a/c}\left[-(a/c)\, V_1 + E_o\, c(1-a^3/c^3) + (a/r)\left\{V_1 - E_o c(1-a^3/c^3)\right\}\right]$$

$$+ E_o\left(r - \frac{a^3}{r^2}\right)\cos\theta. \tag{8}$$

Differentiating Eq. (8) and placing $r = a$ we obtain the radial field at the surface of the sphere, and since under out assumptions the sphere will be at virtually the same potential as the lower plate, we take $V_1 = 0$ and obtain:

$$E_{r=a} = E_o\left\{\left[1 + \frac{c}{a} + \frac{a}{c}\right] + 3\cos\theta\right\} \tag{9}$$

The current entering the sphere will then be

$$I = \int_0^{\pi} \sigma_o E_{r=a}\, 2\pi a^2 \sin\theta\, d\theta$$

$$\therefore I = 4\pi a^2 \sigma_o E_o \left[\frac{7}{4} + \frac{c}{a}\right] \tag{10}$$

where the second term in Eq. (9) has been integrated over the upper hemisphere, and since $\frac{c}{a}$ is generally greater than 10, the first term in Eq. (9) contributes most to the current; only a small error is introduced by ignoring $\frac{a}{c}$.

3. Streamer Tip Radius

We wish to estimate a proper radius for the sphere at the tip of the streamer. A reasonable assumption is that this radius corresponds to the value at which the electric field is high enough for the secondary electrons of the discharge to produce further ionization. While the increased conductivity of the sphere caused by this further ionization will reduce the field, the value obtained from the solution to Laplace's equation will be approximately correct. We therefore write the field intensification α at distance r from the center of the hemispherical cap on the streamer, radius b and height c, by differentiating Eq. (8) as:

$$a = \frac{E_r}{E_o} = \frac{b^2}{r^2}\left(1 + \frac{c}{b} + \frac{b}{c}\right) + \left(1 + \frac{2b^3}{r^3}\right)\cos\theta, \qquad (10a)$$

where $\theta \sim 0$, since the solution ignores the field from the streamer cylinder and considers only that near the tip due to the hemisphere. Taking $\theta = 0$ and solving this equation for $\frac{r}{b}$ we obtain the values shown in Fig. 8 for various values of the intensification. Typically ionization is important for $E_r \sim 3E_o$, and a representative value is $\frac{r}{b} \cong 3$. Identifying the radius with the cap sphere radius a, we may express this quantity from Eq. (10a) in good approximation as:

$$\frac{a}{b} = \sqrt{\frac{1 + c/b}{a - 1}}, \text{ where b/c is neglected,}$$

and since $c/b \gg 1$, we obtain

$$\frac{a}{b} \approx \sqrt{c/b\,(a - 1)} \qquad (11)$$

4. Streamer Temperature

We can now combine Eqs. (5) and (10) and use the above value for a/b to estimate the temperature of a thermally stable streamer column. The expression for the constant becomes:

$$C = \frac{16}{15}\frac{T_o \sigma_o E_o^2}{K_o} \cdot \frac{c^2}{(a-1)^2}\left[\frac{7}{4} + \sqrt{\frac{c(a-1)}{b}}\right]^2 \qquad (12)$$

We note that C depends only slightly on the streamer radius. For a typical discharge in nitrogen, we have c ~ 1 cm; taking b = 1 mm, $T_o = 300^oK$, $\sigma_o = 2.6 \times 10^{-4}$ mho cm^{-1}, $E_o = 5000$ v/cm, and recalling

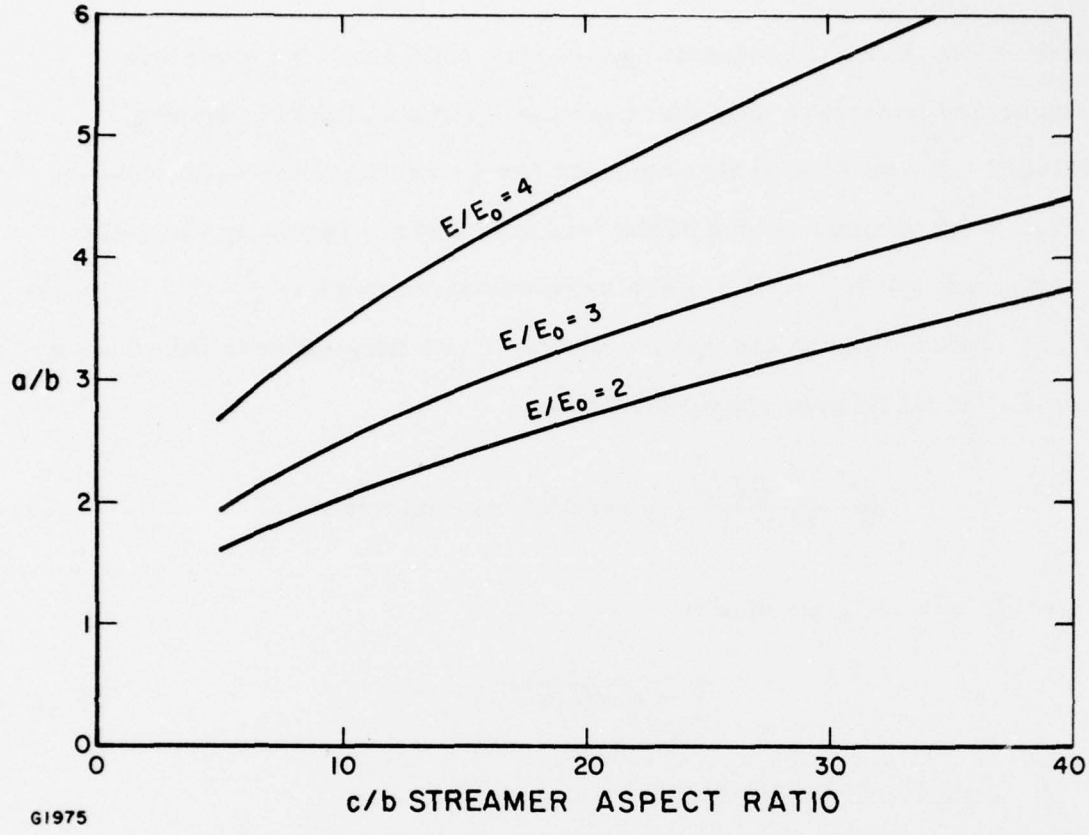

Fig. 8 Ratio of Cap Sphere to Cylinder Radius for Streamers, as Function of Aspect Ratio

that $\kappa_o = 3.145 \times 10^{-10}$, we get $C = 6.4 \times 10^{16}$. From Fig. 7, this corresponds to a temperature $T \approx 6200^{\circ}K$ in pure nitrogen.

Thus we have obtained the temperature at which the streamer column will be stable: we note that it is positively stable since a local increase in temperature will tend to increase electrical conductivity and reduce joule heating, as well as increase the cooling, so that the temperature will be reduced; similarly a local decrease in temperature has the opposite effect.

5. Streamer Radius

The radius b of the streamer is not determined by stability criteria, which merely fix the temperature with respect to current passing through the streamer. We will set a limit on the radius by supposing that the streamer expands radially at a velocity corresponding to the rate of heat diffusion into the ambient gas. The visible streamer will be the gas at temperature near $6000^{\circ}K$, which will also be conducting most of the current. For discharge duration τ, the streamer base radius at the end of the discharge will then be $b \approx \sqrt{\kappa \tau/\rho C_p}$. We note that b will increase as discharge pressure decreases. Taking the values corresponding to $10^3\ ^{\circ}K$ for N_2 we obtain $b \approx \sqrt{4.5\ \tau/N}$, where N is gas density (amagat), and typically in an atmospheric discharge after 100 μsec we obtain $b \approx 0.2$ mm. We expect streamers to be narrower in the shorter, more highly pumped discharges.

6. Streamer Heating at Tip

We will now estimate the rate of heating of the gas in the region of the streamer tip. As this gas is heated it will expand isotropically thus increasing the electrical conductivity, and at high enough temperatures

sufficient thermal ionization will be present to further increase the conductivity.

Since the electrical conductivity must rise very rapidly as r decreases in the sphere, an appropriate model for the conductivity might be $\sigma = \sigma_o' \, e^{ka/r}$ where k is a constant and the conductivity at r = a is the same as that in the undisturbed medium, so $\sigma_o' = \sigma_o \, e^{-k}$. The net heating rate $\dot{q}$ within the sphere is then obtained by integrating j^2/σ over the cap sphere, down to a radius corresponding to the cylinder radius. We obtain:

$$\dot{q} = \int_b^a \frac{I^2}{(4\pi r^2)^2} \, 4\pi r^2 \, \frac{e^{-ka/r}}{\sigma_o'} \, dr.$$

This is integrated by substituting $p = \frac{1}{r}$, and we obtain

$$\dot{q} = \frac{I^2}{4\pi\sigma_o \, ak} \left[1 - e^{-k(a/b - 1)} \right] \cdot \text{ watts}$$

Noting that the ratio of conductivities at 6200°K and 300°K is approximately 10^3, allowing for the external ionization, and taking the value a/b = 3, we obtain k = 3.45. Thus the second term in the expression for $\dot{q}$ can be ignored, and the mean volumetric heating rate over the sphere is:

$$\dot{q}_s = \frac{3I^2}{16\,\pi^2 \, \sigma_o a^4 k} \cdot \text{ W/cm}^3 \qquad (13)$$

This result does not depend strongly on the model chosen for the conductivity, for if instead we write $\sigma = \sigma_o (r/a)^{-m}$, where m is a constant,

in order to represent the rapidly increasing conductivity as the radius diminishes, we can integrate j^2/σ over the sphere and average it as before, and we obtain:

$$\dot{q}_s = \frac{3I^2}{16\,\pi^2\,\sigma_o\,a^4(m-1)}$$

in place of Eq. (13). For the same range of temperatures, conductivities and radii we find m = 6.29; the ratio of the two volumetric heating rates is then 3/2 approximately, so that the determination of $\dot{q}_s$ is close to model-independent. In the subsequent work we will use that given by Eq. (13).

We have ignored radial temperature differences due to variation of heating rate radially within the sphere; in actual fact only the central region will reach the cylinder temperature derived in Eq. (5), and we are over-estimating the energy required to do so. An approximate estimate of the magnitude of the correction for the fact that the temperature varies inversely with radius in the sphere may be made as follows. We have written the electrical conductivity as $\sigma = \sigma_o\, e^{k(a/r-1)}$ in Eq. (12), and shown that the volumetric heating rate is relatively model-independent. It is a good approximation for the temperature dependence of conductivity in the region $T > 6000^o$ to write $\sigma = \sigma_o(e^{T/T_2} + 1)$, where $T_2 \approx 898^o K$ and a base conductivity σ_o is provided by external ionization. The self-consistent variation of temperature with radius is then

$$T = k\,T_2\,(a/r-1).$$

The volumetric heating needed to bring the center of the sphere to the critical temperature T at which it becomes sufficiently conductive to support the streamer cylinder is then:

$$\langle\eta\rangle = \frac{1}{V}\int_b^a 4\pi\, r^2\, \epsilon_o\, (T/T_1)^\gamma dr$$

where V is the sphere volume and $\gamma = 0.63$ for a nitrogen discharge (see Appendix A). Making the substitution and comparing this value with the volumetric heating η needed to bring the entire sphere to the temperature T, we obtain the correction factor

$$\lambda = \frac{\langle\eta\rangle}{\eta} = 3\left(\frac{kT_2}{T}\right)^\gamma I(b/a),$$

where

$$I(b/a) = \int_{b/a}^1 x^2(1/x-1)^\gamma\, dx.$$

Numerical integration of I taking $\gamma = 0.63$ is given in Table I, showing that I is a slowly varying function of b/a, and for $b/a = 1/3$ we obtain $I = 0.158$. For $k = 3.45$, $T_2 = 898^\circ K$, $T = 6200^\circ K$, we have $\langle\eta\rangle/\eta = 0.30$. We conclude that ignoring the temperature distribution in the sphere will result in calculated heating that is too large and should be reduced by a correction factor $\lambda = 0.3$.

TABLE I

NUMERICAL INTEGRATION

b/a	I	$\lambda = \langle\eta\rangle/\eta$
0.1	0.180	0.349
0.2	0.175	0.339
0.3	0.163	0.316
0.333	0.158	0.306
0.4	0.146	0.283
0.5	0.124	0.240

7. Streamer Velocity

At this point we can identify a characteristic velocity for propagation of the streamer. It is the radius of the sphere divided by the time taken to reach the stable streamer temperature obtained above. Using the Air Force values [6] for the enthalpy of N_2 (see Appendix A), we can write the energy required to bring 1 cc of gas at 1 atm from 300°K to temperature T as:

$$\epsilon = \epsilon_o (T/T_1)^{0.63}$$

where $T_1 = 3500^\circ K$, $\epsilon_o = 1$ joule/cm^3. In the present model, the mass of gas heated is continuously diminished as it expands outward past r = a and leaves the region of heating; we can ignore the conductive heat loss compared to this large convective heat loss, which is automatically included in the expression for ϵ, and the total volumetric heat input under these conditions will be:

$$Q = \epsilon N \lambda \qquad (14)$$

where N is gas density normalized to 1 atmosphere, taking initial temperature as 300°K.

Identifying this energy with the heat input gives the heating time τ:

$$\tau = Q/q_s.$$

Writing the streamer velocity as $v = a/\tau$ and collecting terms we obtain the velocity as:

$$v = \frac{3\, a\, \sigma_o\, E_o^{\,2}}{\lambda\, k\, \epsilon\, N} \left[\frac{7}{4} + \frac{c}{a}\right]^2 \qquad (15)$$

For a typical discharge in nitrogen, taking the values $a = 0.4$ mm, $\sigma_o = 2.6 \times 10^{-4}$ mho cm^{-1}, $E_o = 3500$ V/cm, $c = 0.5$ cm, $\lambda = 0.3$, $\rho_o = 1.12 \times 10^{-3}$ g/cm^3, $T_1 = 3500^\circ$K, $T = 6200^\circ$K, $k = 3.45$ we get

$$v = 1.5 \times 10^4 \text{ cm/sec}$$

and we note that the sound speed in the undisturbed gas is $v_c = 3.53 \times 10^4$ cm/sec, so that in this case the streamer travels at less than Mach 0.5, implying that the assumption of uniform pressure is still consistent with the predicted velocity.

For velocities below Mach 1 the assumption that the gas expands rapidly enough so that the expression for the energy input per unit volume required to reach temperature T, $\epsilon_1 = \int_{T_o}^{T} \rho C_p\, dT$ where gas density ρ is a function of T, will be approximately valid. In this region the constant volume enthalpy discussed in Appendix A should be used in calculating the velocity from Eq. (15).

At supersonic speed, however, the gas cannot expand rapidly enough during the heating process, and the gas density will remain close to its initial value ρ_o during heating. The energy input per unit volume is then

$\epsilon_3 = \rho_o \int_{T_o}^{T} C_v \, dT$, and the streamer velocity must be calculated based on the internal energy. Since the density is still at the initial value, $\epsilon_3 \gg \epsilon_1$, and the discharge power loading into the streamer must be correspondingly greater in order to make the streamer propagate supersonically.

In the intermediate region the energy input ϵ_2 per unit volume required to reach temperature T has an intermediate value, or $\epsilon_1 < \epsilon_2 < \epsilon_3$. While we do not know exactly how this energy is distributed between gas internal energy and gas kinetic energy, we do know that the resultant streamer velocity must be Mach 1. Thus we can distinguish subsonic sonic and supersonic regimes of streamer propagation. Since the power loading into the streamer increases as it moves across the discharge, we expect these regimes to succeed each other in sequence.

The subsonic regime is considered in the discussion above leading up to Eq. (15). This equation will be taken as valid with $\epsilon = \epsilon_1$ until the velocity equals the soundspeed in the undisturbed medium, a point we identify as $c = c_1$. After this point the velocity will be assumed to remain at the soundspeed until the streamer has reached a length $c = c_3$, at which the velocity begins to become supersonic. As the streamer further increases in length the velocity will continue to increase. Since the only physics altered is the value of ϵ, Eq. (15) can still be used to derive the supersonic velocity, placing $\epsilon = \epsilon_3$. There is a small change to be made in the value of λ; in the case of nitrogen at 1 amagat the internal energy may be suitably approximated as $\epsilon_3 = \epsilon_o e^{T/T_4}$, where $\epsilon_o = 0.596$ j cm^{-3} and $T_4 = 2010^{\circ}$K. We may then derive λ as before and obtain

$$\lambda_3 = \frac{3e^{-(T + kT_2)/T_4}}{1 - b^3/a^3} \int_{b/a}^{1} x^2 e^{k T_2/(T_4 x)} dx \qquad (16a)$$

where $k = 3.45$, $T = 6200^{\circ}K$ and $T_2 = 898^{\circ}K$, and we define λ_3 as the supersonic value of λ. Taking $b \approx a/3$, as we did in the previous case, and evaluating Eq. (16a) we obtain $\lambda_3 \approx 0.105$, which will be used below.

We may now use Eq. (15) to determine the boundaries c_1 and c_3 of the sonic regime. In order to do this we must identify the value of the core radius b in the head region of the streamer. We will assume that this is the propagation distance of the conduction heat wave during the time the discharge head moves through its radius, keeping in mind the fact that the gas in the central region of the capsphere will be at the stable streamer temperature, $6200^{\circ}K$ for N_2. Thus

$$b = \sqrt{\frac{\kappa a}{\rho C_p V}} \text{ , where V is the streamer velocity.} \qquad (16b)$$

Combining this with Eq. (11) we obtain the expression

$$a = f\, c^{2/3} , \qquad (16c)$$

where $f = \left[\frac{\kappa/\rho C_p V}{(\alpha-1)^2}\right]^{1/3}$, and substituting in Eq. (15) the velocity may be written

$$\frac{dc}{dt} = A_i f\, c_i^{2/3} \left[7/4 + \frac{c_i}{f}^{1/3}\right]^2 \qquad (17a)$$

where $A_i = 3\sigma E_o^2/(\lambda_i k \epsilon_i)$, and i = 1 or 3 for the subsonic and supersonic limits of the sonic regime, respectively. For a nitrogen discharge we take f = 0.055 [since V is present to the 1/3 power it is a slowly varying factor and we can take V = soundspeed], and identifying $\frac{dc}{dt}$ with the soundspeed we can solve Eq. (17a) for the limits c_1 and c_3. These are given in Table II for a nitrogen discharge at atmospheric pressure and 300°K. For typical loadings near 3 kW/cm^3, the streamer will move at sonic velocity between 0.3 and 1.4 cm, thereafter becoming supersonic. Streamer behaviour as a function of time will be discussed in the next section.

TABLE II

STREAMER SONIC LIMITS

$\sigma_o E_o^2$ W cm^{-3}	c_1 cm	c_3 cm
10^3	0.84	3.43
3×10^3	0.34	1.39
10^4	0.134	0.57
3×10^4	0.06	0.24
10^5	0.02	0.09

Finally we notice that the initial value of b at the electrode, b_o, may be estimated by taking $b_o = c$ and $V = \frac{dc}{dt}$; combining Eqs. (16b), (16c) and (17a) yields the transcendental equation:

$$b_o \approx \left(\frac{\kappa/\rho C_p}{A_1 f\sqrt{a-1}} \right)^{3/5} \left[\frac{7}{4} + \frac{b_o}{f} \right]^{1/3}{}^{-6/5} \qquad (17b)$$

For an atmospheric pressure N_2 discharge we find the values for b_o in Table III. We take as the value corresponding to a typical discharge $b_o = 0.016$ cm.

TABLE III

STREAMER RADIUS

$\sigma_o E_o^2$ W cm^{-3}	b_o cm
10^3	2.9×10^{-2}
3×10^3	1.8×10^{-2}
10^4	1.0×10^{-2}
10^5	3.4×10^{-3}

8. Growth of Streamers

The length of a streamer for $c < c_1$, or for $c > c_2$ will be given by integration of Eq. (17a) between appropriate limits, writing $c_i = c$. In the intermediate region the streamer will move at the soundspeed. We consider the three regimes separately.

a) Subsonic Regime

The lower integration limit is the minimum radius at the electrode, b_o, and the upper is distance D_1 from the electrode, with the condition $D_1 < c_1$. We have

$$\int_{b_o}^{D_1} \frac{c^{-2/3}}{f} \left[\frac{7}{4} + \frac{c^{1/3}}{f}\right]^{-2} dc = A_1 \tau_1, \tag{18a}$$

where τ_1 is elapsed time. This becomes:

$$\tau_1 = \frac{3}{A_1\left[\frac{7}{4} + \frac{b_o^{1/3}}{f}\right]} \cdot \left[\frac{1 - (b_o/D_1)^{1/3}}{1 + 7f/(4D_1^{1/3})}\right] \tag{18b}$$

The transition to the sonic regime occurs at the limit $D_1 = c_1$

b) Sonic Regime

In the intermediate regime the velocity is sonic, and

$$\tau_2 = (D_2 - c_1)/V_s, \tag{18c}$$

where D_2 is distance from electrode and V_s is soundspeed, and $c_1 < D_2 < c_3$.

c) Supersonic Regime

The integration limits are now c_3 and D_3, and

$$\int_{c_3}^{D_3} \frac{c^{-2/3}}{f} \left[\frac{7}{4} + \frac{c^{1/3}}{f}\right]^{-2} dc = A_3 \tau_3 \tag{18d}$$

Integration yields:

$$\tau_3 = \frac{3}{A_3\left[\frac{7}{4} + \frac{c_3^{1/3}}{f}\right]} \left[\frac{1-(C_3/D_3)^{1/3}}{1 + 7f/(4D_3^{1/3})}\right] \tag{18e}$$

with the condition $D_3 > c_3$.

Equations (18b), (18c) and (18e) now give us the length of time taken for the streamer to reach any given length. Formally speaking it can be see from (18e) that the streamer will cross any discharge in a finite time; letting $D_3 \to \infty$ yields $\tau_3 \to 3/[A_3(7/4 + c_3^{1/3}/f)]$. The history of streamer length in an atmospheric pressure nitrogen discharge is shown as function of elapsed time in Fig. 9 for discharges at various power loadings. It is apparent that the sonic regime occupies a relatively constant fraction of the total duration. We would expect streamers to traverse relatively large discharges 30 cm across almost as rapidly as those only 5 or 10 cm across. Since the discharge arc initiates according to the present hypothesis when the streamer has traversed the discharge cavity, we expect the advantage in arcing limit gained by large discharge electrode spacing to be very small. Predictions of arcing limits and comparison with experiment will be given below.

9. Streamer Scaling

It is interesting to note that in the subsonic regime the transit time given by Eq. (18b) is essentially the constant-pressure energy required to heat the gas up to temperature T given by Eq. (5) divided by the rate of heat input. If E/N is kept constant and the gas density N is varied, for most applications of the non-self-sustaining discharge it is kinetically favorable to maintain n_{eo}/N constant, which results in unchanged pumping rate per molecule. The electrical conductivity will then be independent of gas density, and τ scales as

$$\tau = K \frac{\epsilon}{\sigma_o (E_o/N)^2 N} \qquad (19a)$$

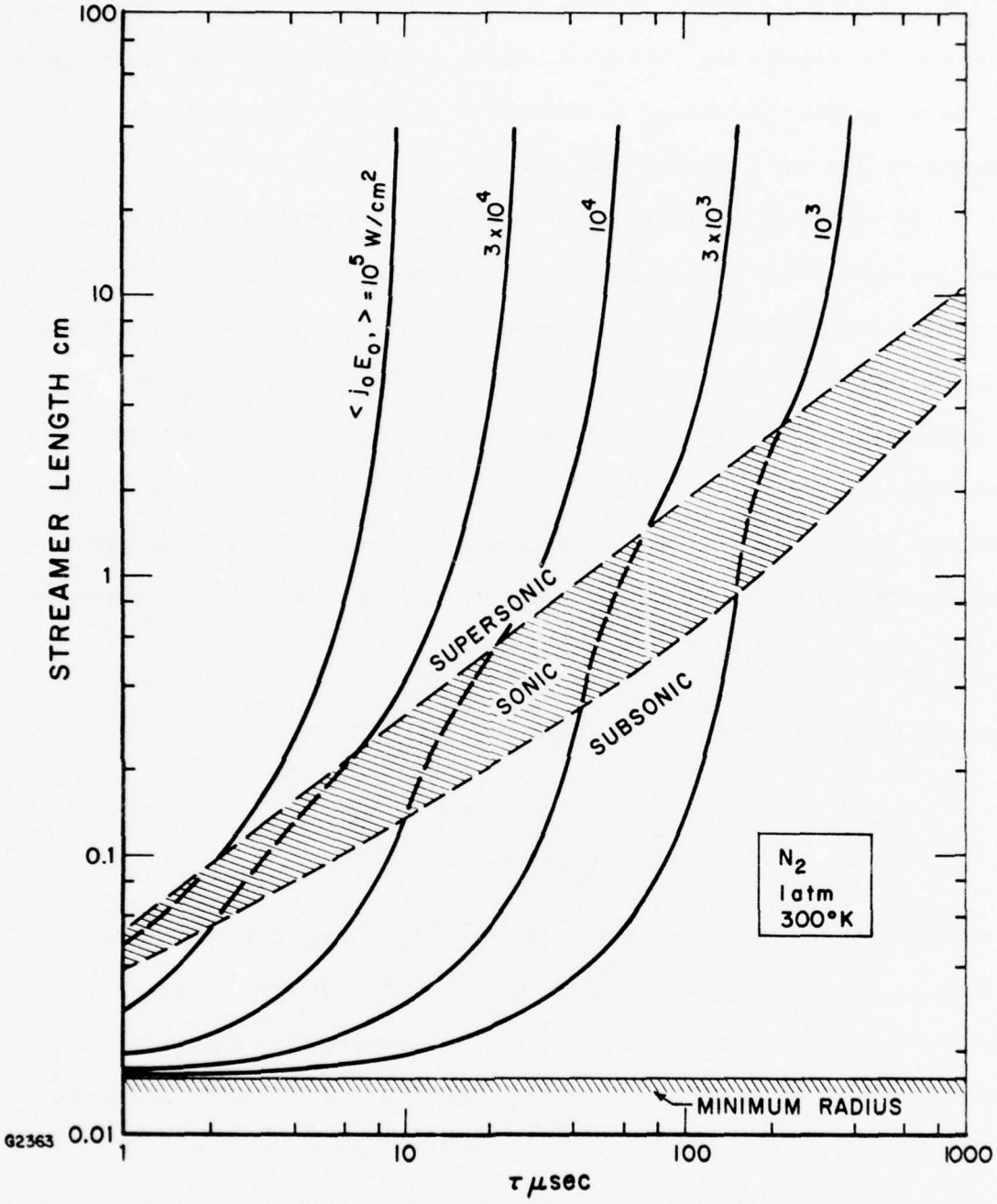

Fig. 9 Streamer Length vs Time

so that arcing time varies inversely with gas density, which is consistent with the observation that EB sustainer discharges in gases at low pressures arc less readily than at high pressure for the same E/N. The same scaling applies for the time spent in the supersonic regime.

In practical discharges the streamers are likely to reach the sonic or supersonic regimes before completing their journey. We note that since the soundspeed is independent of gas density low pressure discharges of the CW type are less likely to attain the supersonic regime, and therefore will take longer to arc, than high pressure discharges. The values of c_1 and c_2 have been computed from Eq. (17a) for the gas mixture He: N_2: CO_2 3: 2: 1 at various pressures and power loadings, and are shown in Fig. 10. Equation (17a) reduces fairly accurately to the expression $c_i \simeq \left(\frac{f_o c}{A_i}\right)^{3/4} N^{1/4}$, since $f = f_o N^{-1/3}$, and thus the duration of transit of the sonic regime varies as

$$\tau_2 \propto \left(\frac{1}{\sigma(E/N)^2}\right)^{3/4} N^{-1/2} \qquad (19b)$$

Consequently the lower the pressure, the longer the relative duration in the sonic regime. The variation of transit time τ with power loading $\sigma_o E_o^2$ in the sonic case is not quite as fast as in the subsonic and supersonic cases, both of which follow Eq. (19a), thus leading to slight variations from the straightforward concept of a limiting permissible discharge loading energy. Predictions will be made for various discharges below.

10. Summary

The streamer model developed above derives a streamer velocity proportional to the square of the discharge electric field in the subsonic

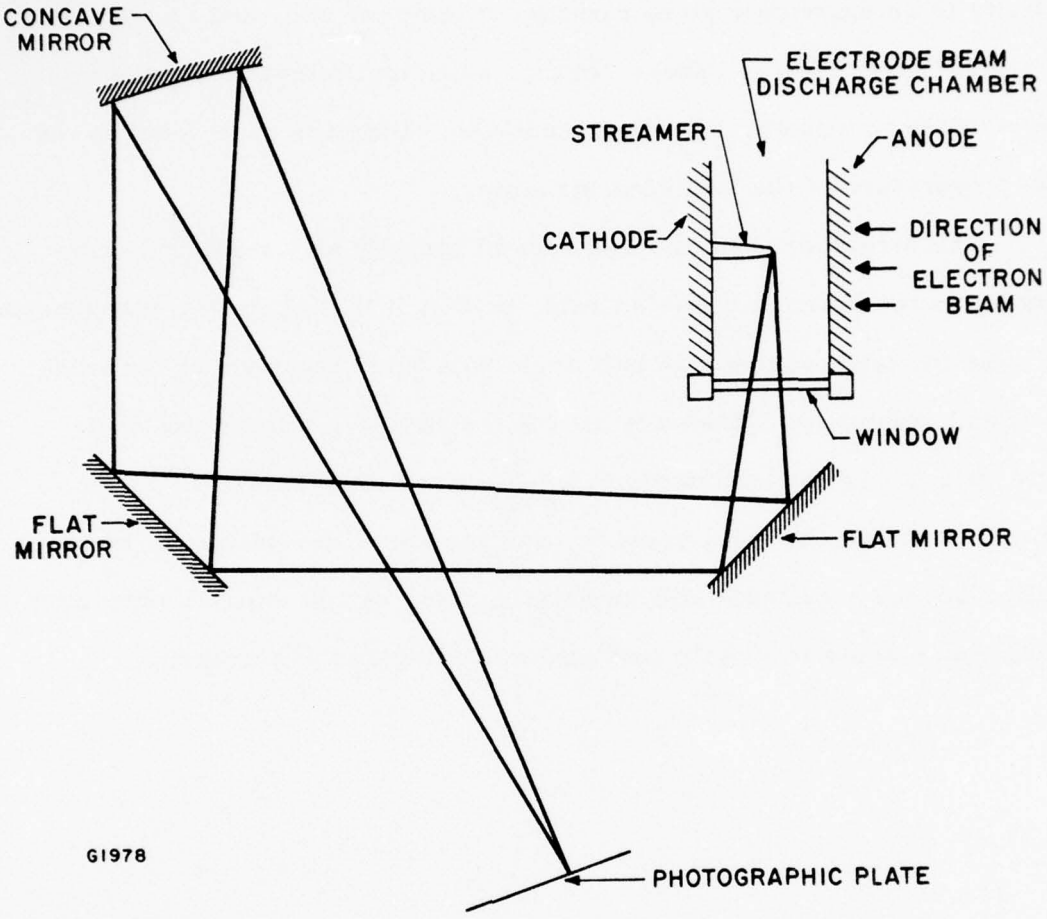

Fig. 10 Schematic of the Optical Arrangement Used for Photographing Streamers

regime. After a sonic transition, at high fields the predicted velocity will be supersonic and the assumption of uniform pressure will be invalid, resulting in corrections to the thermal equations. The electrical conductivity is an extremely steep function of temperature, and as soon as the central region of the sphere reaches sufficient temperature the ionization region moves on, ingesting fresh gas. Only the core reaches the high temperature of the luminous streamer.

The streamer cylinder will expand radially at a velocity corresponding to the thermal diffusion rate, so that it will acquire the appearance of a cone the tangent of whose half angle will equal the ratio of the axial and radial velocities. However, taking the radius $b = 0.05$ cm, the radial velocity is approximately $v \approx \frac{\kappa}{\rho C_p b} \approx 90$ cm/sec for N_2, which is much less than the axial velocity, and the above derivation of thermal equilibrium for a cylinder will be satisfactory. Approximately speaking, arcing times scale inversely with power loading and gas pressure.

III. EXPERIMENTAL RESULTS

A. PRELIMINARY CASES

An electron-beam sustainer discharge device was used to produce streamers in a nitrogen discharge at atmospheric pressure. The device, which has been described previously,[7, 8] is shown schematically in Fig. 1. A 90 kV electron beam enters the chamber through a 1/2 mil aluminum foil and an electrode plate perforated with 1/8 inch holes in a 5 x 10 cm rectangular array; it ionizes the gas present and a discharge then takes place in the secondary electrons between the perforated plate and the second electrode; discharge spacing is 2.54 cm. The second electrode consists of a lucite plate with grooves in which stainless steel rods of various diameters can be placed. These rods are electrically connected to the sustainer capacitor. An optical arrangement of two flats and a 325 cm radius mirror (see Fig. 10) images streamers on a photographic plate (Polaroid High Speed Type 57, rating ASA 3000), arranged so as to produce a slightly demagnified image with magnification m = 0.92.

Experiments consist of filling the discharge chamber with selected gas and firing the discharge, photographing the streamers generated on the rods while they move across the discharge.

Since we do not have time discrimination within the discharge pulse, photographs are prepared for successively longer pulse duration until the discharge arcs. When this happens the photograph is totally overexposed.

1. Rods Parallel to the Optic Axis

Three rods were used in this experiment, placed in the lucite electrode holder from left to right with diameters 0.16 cm, 0.24 cm and 0.32 cm respectively, and using it as cathode. The streamers produced

for discharges of different duration in nitrogen, using applied electric field E_o = 2600 V/cm and electron density $n_{eo} = 10^{12}$ cm^{-3}, are shown in Fig. 11; the rods increase in size from left to right, the smallest rod producing the largest streamer as might be anticipated. The rectangular aperture in the perforated plate is placed with its long axis normal to the optic axis so as to locate the streamers as near to the focal plane as possible, while the rods are parallel to the optic axis. It is immediately evident that the streamers from the thinnest rod have propagated most rapidly across the discharge, as well as achieving the greatest geometric complexity. They tend to follow the field lines, and we note that the field distortion at the rods is so great that rod position is more important than rod radius in determining streamer growth rate. Nonetheless we can estimate a growth rate from Fig. 11; we get a slowly increasing streamer velocity of ~ 1.5×10^4 cm/sec.

2. Rods Perpendicular to the Optic Axis

Since the streamers in the previous case are following rather complicated field lines, their velocity is not very well defined, and a more uniform field would be desirable. The rectangular EB window and the cathode rods were rotated 90°, and in addition the two outer rods were removed and the lucite electrode holder was covered with aluminum foil to provide a uniform electric field in the discharge. The central rod provided a discontinuity on which streamers were likely to form, and the apparatus was adjusted so that the focal plane lay along the central rod.

A typical series of shots is shown in Fig. 12a. These were performed in nitrogen at atmospheric pressure, with E_o = 2640 V/cm and $n_{eo} = 10^{12}$ cm^{-3}. A halo region is visible around the streamer tip, as

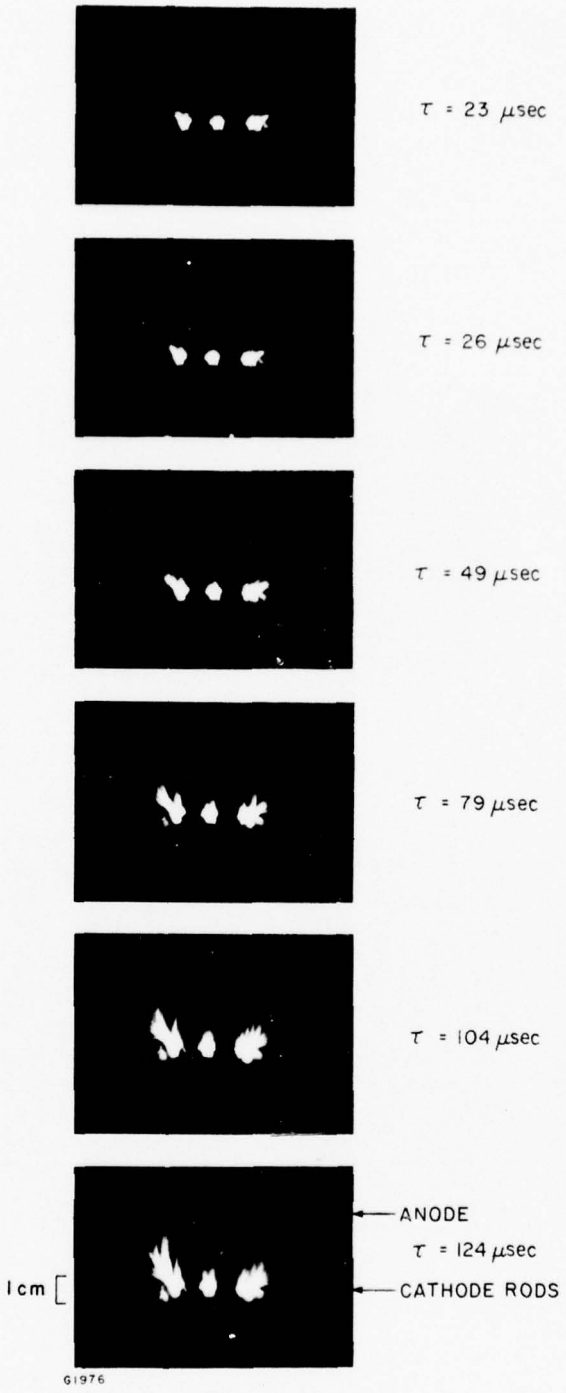

Fig. 11 Streamer Growth; Three Cathode Rods Parallel to Optic Axis

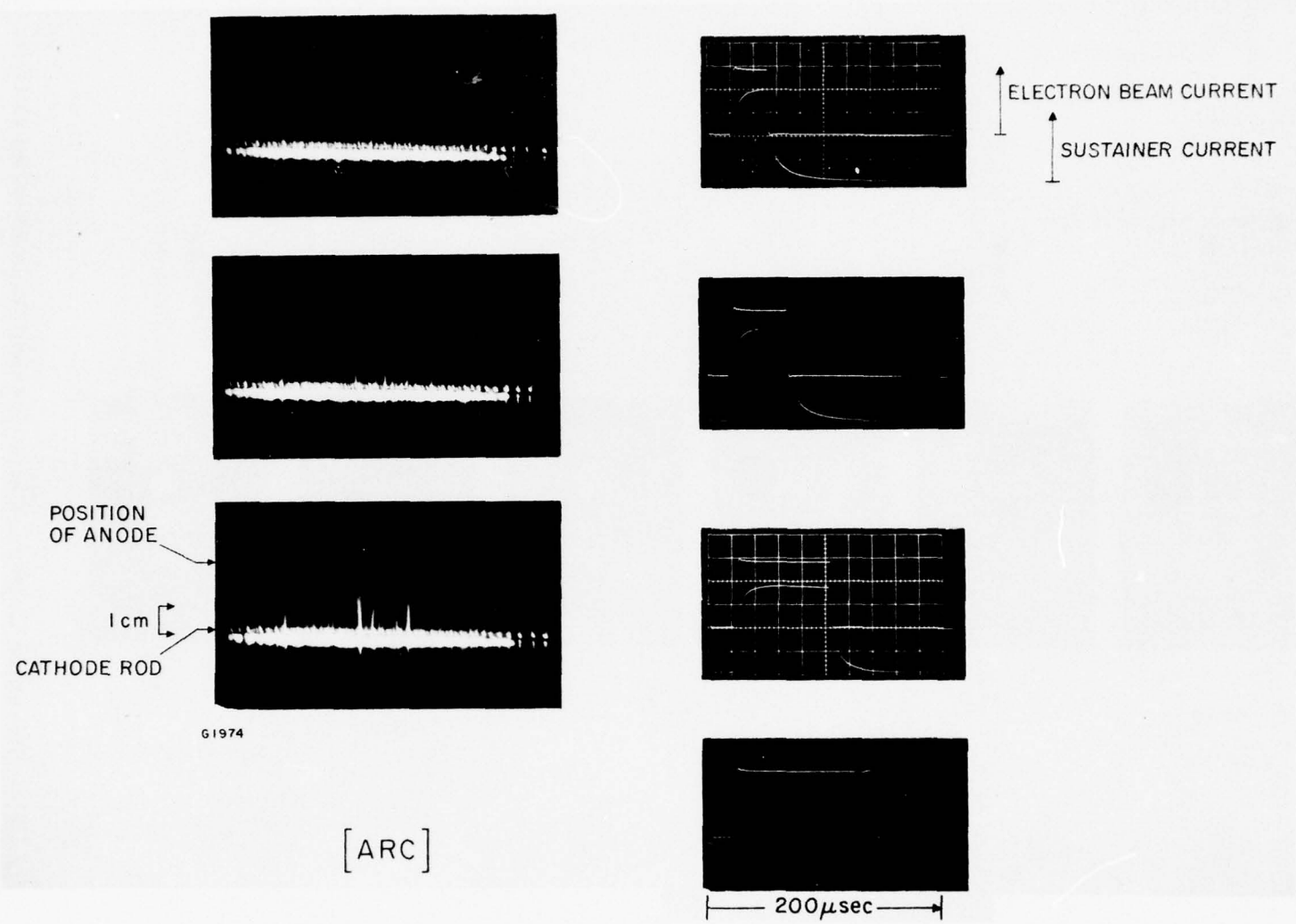

Fig. 12a Streamer Growth; Single Cathode Rod Perpendicular to Optic Axis

expected in the model discussed above, in which it corresponds to the region within which secondary ionization is important. The streamer length c is plotted vs time as the dotted line in Fig. 12b, in which it can be seen that the streamer is accelerating across the discharge gap. We will discuss this further below.

The intensity of the image enables us to estimate the temperature of the streamer plasma. The fluence at the image plane, neglecting losses, will be:

$$I_{image} = \frac{a^2}{4m^2R^2} \frac{\pi bE}{2} \text{ J/cm}^2$$

where a is concave mirror stop radius, m is magnification, R is distance from source to concave mirror, E is energy radiated from streamer in joules per cm^3, and b is a characteristic dimension of the streamer (we take the radius). We note that the fluence required to produce 10% increase in density above background on film is $F = \frac{1.18}{S}$ erg/cm^2, where S is the ASA number, at $\lambda = 5550$ Å. A lower limit to the streamer energy radiated, which completely exposes the film, is then $I_{image} \simeq 10F$, which gives

$$E = \frac{8m^2R^2}{\pi a^2 b} \frac{1.18 \times 10^{-6}}{S} \text{ J/cc.}$$

Taking m = 0.94, b = 0.1 cm, a = 10 cm, R = 312 cm, S = 3000, we get $E = 8.6 \times 10^{-6}$ J/cm^3, or for exposure ~ 5 μsec, at tip, $\dot{E} = 1.72$ watt/cm^3.

Using the tables for radiation from heated air,[9] which will approximate that for N_2, we observe that this radiation corresponds to a streamer

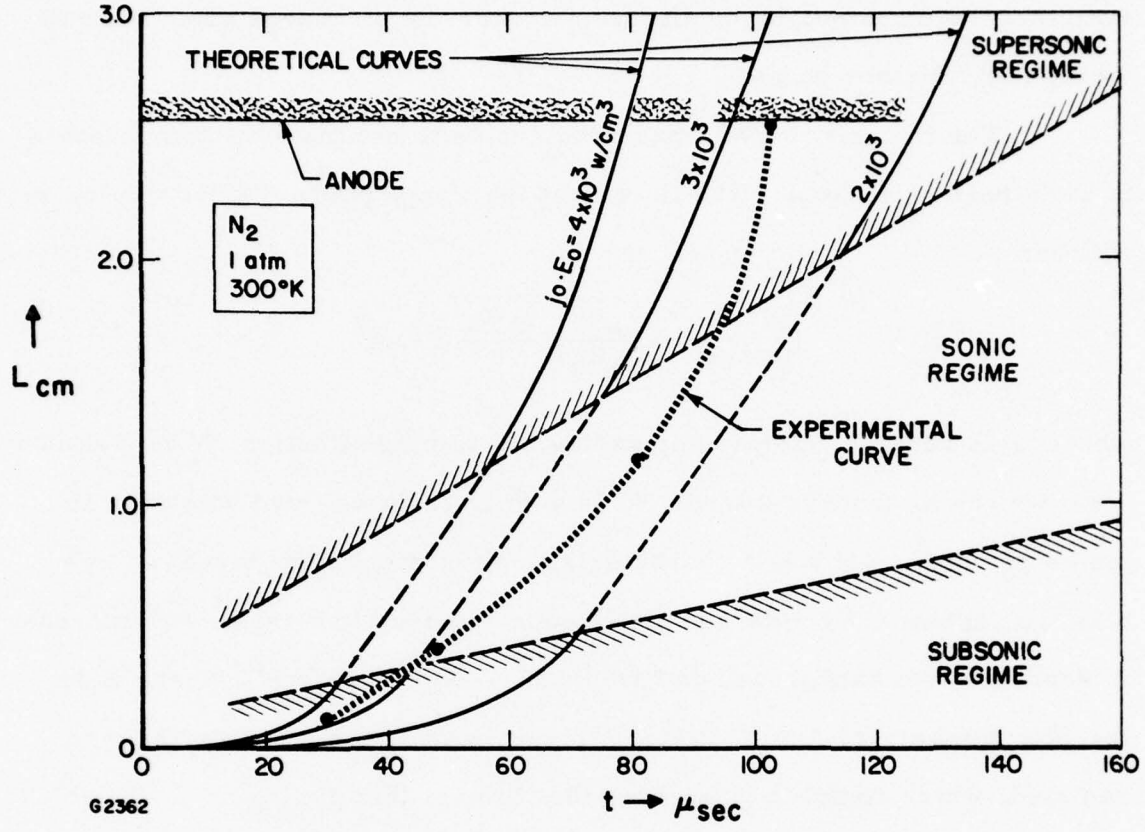

Fig. 12b Experimental and Theoretical Streamer Length

temperature $T \geq 6000^{\circ}K$. Taking the halo as $\sim 10\%$ of this radiation implies a halo temperature $T \sim 4000^{\circ}K$. We note that the Wien blackbody radiation peak occurs at 4800 Å and 7244 Å for these two temperatures, so that using the above estimate for fluence on the film is approximately self consistent. Thus, the streamer appears to have a temperature close to that required by the consideration of heat balance in the foregoing model.

B. FRAMING CAMERA EXPERIMENTS

Recently, we have obtained much more precise data about streamers in our discharge by using a high speed framing camera to record successive stages in the development of a single streamer. This camera, which has a maximum framing rate of 44,000 frames per second is shown in Fig. 13 mounted to view the discharge through a window in the bottom of the cell. The camera was aligned to photograph a narrow strip of discharge extending from the cathode to anode. To ensure that the largest streamer would form in the region observed, a loop of fine tungsten wire was affixed to the cathode at that point. In this way, we were able to observe the development of cathode streamers, as can be seen from Fig. 14, which shows a typical framing sequence.

Data obtained from successive photographs of a single streamer is of course more accurate than that obtained from integrated photos of successive shots, and the framing camera also permits us to photograph streamers which lead to arcing. (In Fig. 14, the last few frames were slightly fogged by the subsequent arc.) The framing camera has also greatly increased our rate of data acquisition, since one shot now provides as much data as did many shots under the old procedure.

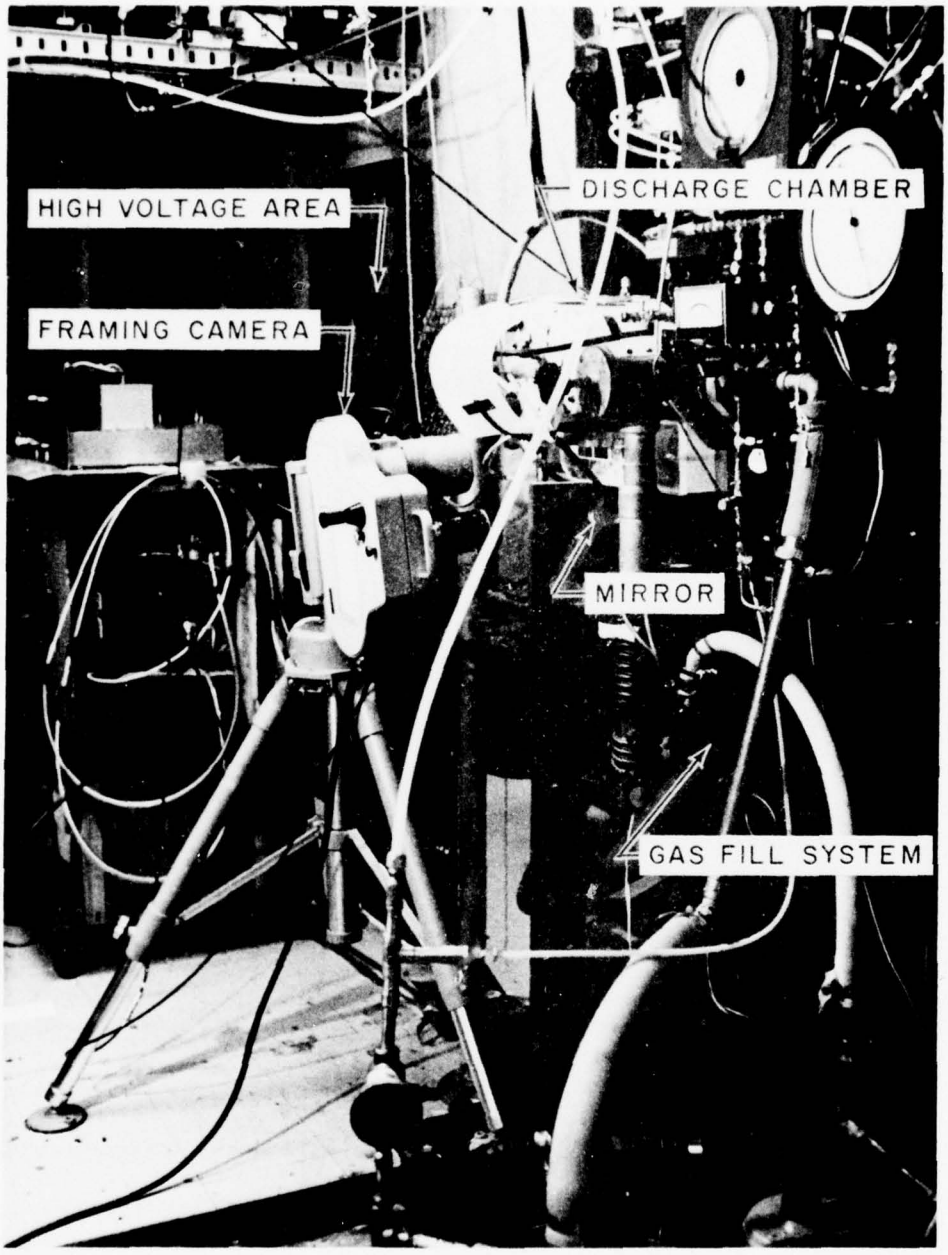

Fig. 13 Experimental Apparatus Including the High-Speed Framing Camera used to Photograph Streamers

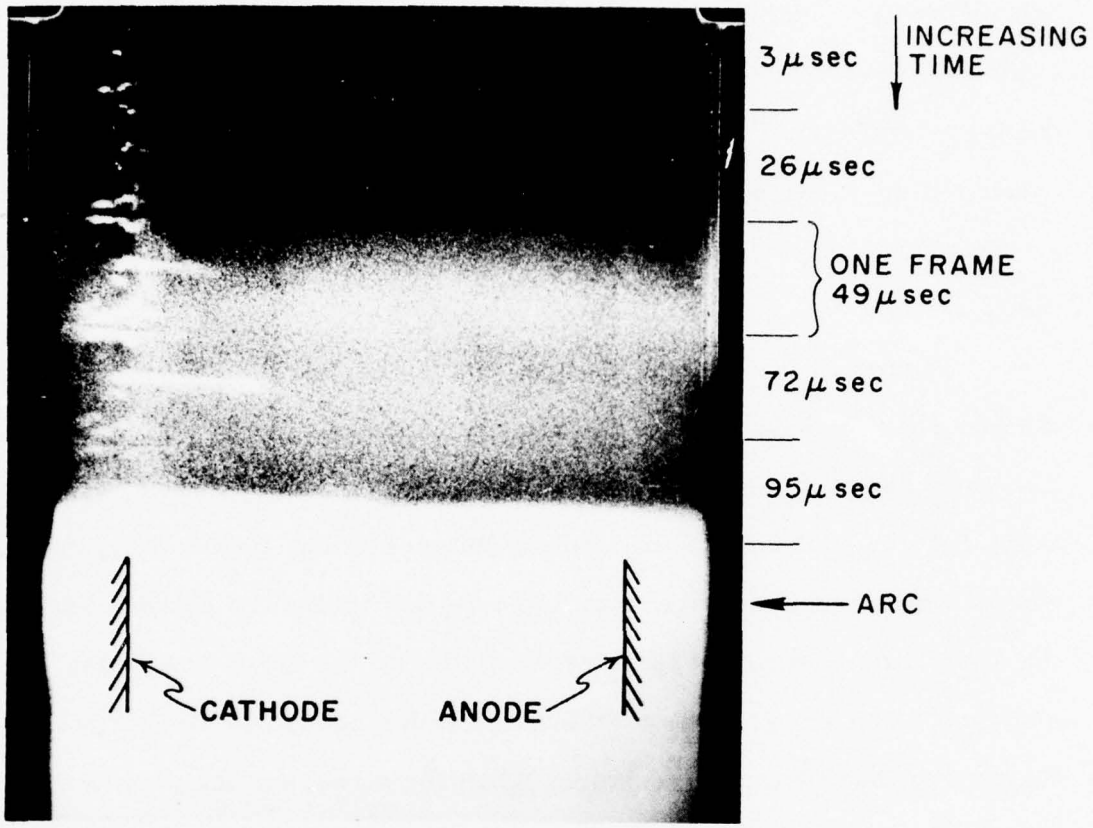

H1278

Fig. 14 Framing Camera Photo Sequence Showing Propagation of a Cathode Streamer and Resultant Arcing When the Streamer Reached the Anode

Time Between Successive Frames	23 μsec
Discharge Medium	N_2, 760 torr
Sustainer Field	4.5 kV/cm
Discharge Current Density	1.97 A/cm^2
Time to Arc	108 μsec

The streamer photographs in Fig. 14 agree quite well with the model in Fig. 4. The streamer does indeed have the form of a cylinder with a ball on the end. (The ball is barely visible in Fig. 14; it is more clearly visible in other framing sequences. The ball is always seen when the exposure is sufficient.) The framing photographs were the first experimental confirmation of these predicted details of the streamer structure, and the evident agreement with the model is a significant confirmation of the assumptions.

Figure 15 is a plot of the data in Fig. 14. As can be seen, within the accuracy of these measurements, the streamer growth is exponential. The occurrence of an arc corresponds to the streamer reaching a length of about 1.5 cm. (The anode to cathode distance is one inch.) This behavior, which is quite reproducible, may indicate that ionization extends beyond the visible streamer, but is more likely due to the onset of a faster instability. The streamer is a slow mode which occurs in discharges below the conventional arcing threshold. When the streamer has propagated more than halfway across the medium, a very strong field is produced between the streamer tip and the anode, exceeding the threshold for rapid breakdown of the remaining segment of the path needed for an arc.

The streamer appears to start with a length of about 1 millimeter. In Fig. 14, this may merely represent the size of the wire loop on the cathode, but since the arcing time in this discharge is not greatly changed by the addition of the wire, streamers of this size apparently form rapidly at the cathode in any case.

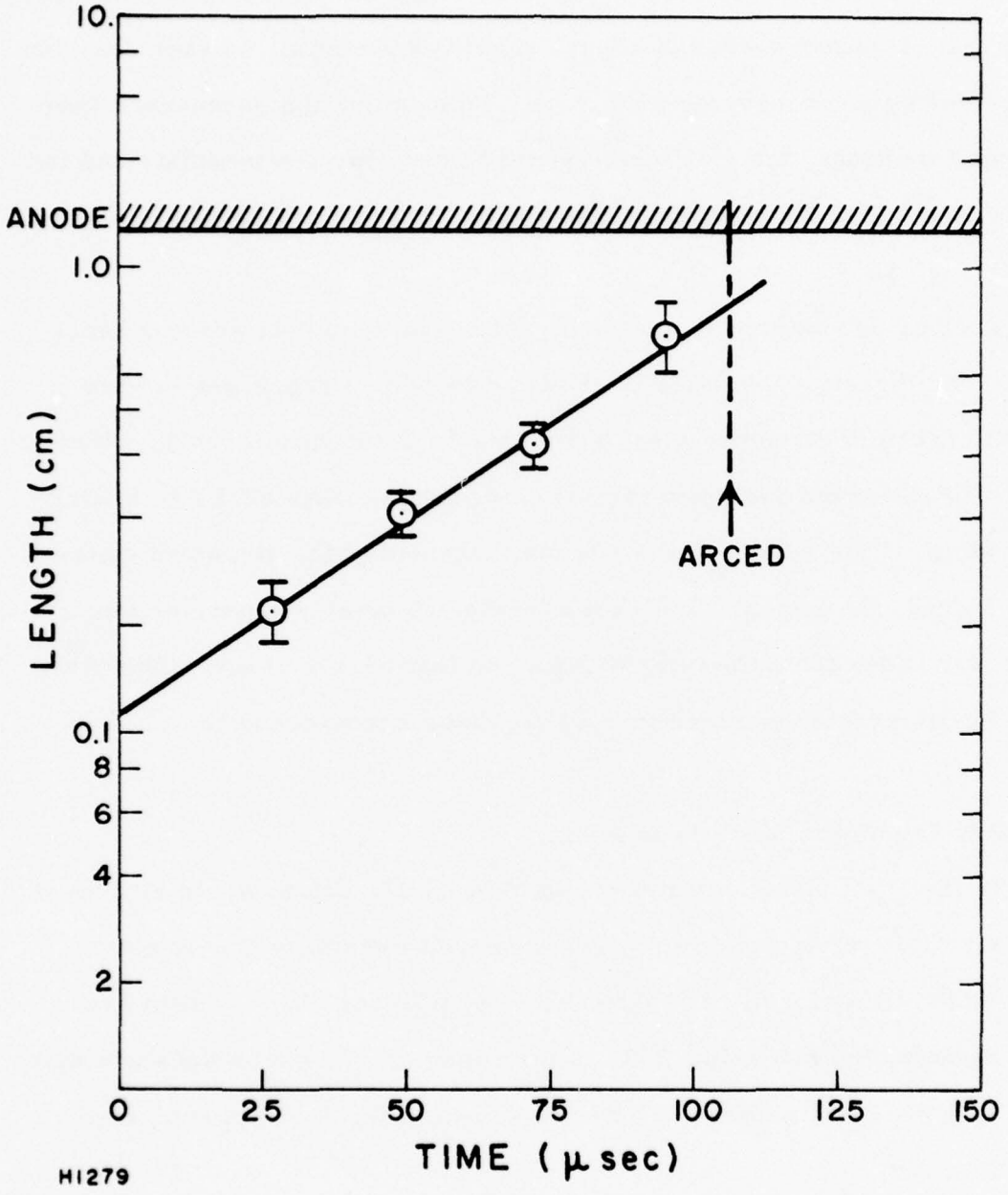

Fig. 15 Growth of the Streamer Shown in Fig. 14

Data like those in Fig. 14 were taken over a wide range of discharge currents and electric fields* (but, only in nitrogen at atmospheric pressure.) We find that streamer growth is always nearly exponential, so each shot can be described by an observed growth rate. To examine the dependence upon discharge conditions, the data were grouped into slow, intermediate and fast growth cases. The distribution of these points in the current-power plane is shown in Fig. 16.

A clear dependence is apparent. Although the points cover a range of more than threefold variation in growth rate (which represents a very large difference in streamer size, since this is exponential growth, which we typically observed over several E-folding times), they all lie in a fairly narrow strip. This region in P - j is the threshold of the streamer instability. Indeed, the straight line shown in Fig. 16 cleanly separates the slow growth cases from the intermediate and fast growth cases. This line, which is quite precisely determined by the data, corresponds to

$$P - 3.8\, j = 1$$

where P is in kW/cm^3 and j is in A/cm^2.

In the P - j plane, a straight line through the origin would represent a constant value of electric field. The observed instability line is almost, but not quite of this form. The difference is apparent when the data are plotted against electric field. This is done in Fig. 17, where the same data points, and the same separation line are shown in the P - E plane. Here

*The electric field is set by the applied voltage; the current is determined by this and by the e-beam current, which can be independently selected. Thus, there are two electrical parameters, which can be variously stated, e.g., current and electric field, or current and power density, etc.

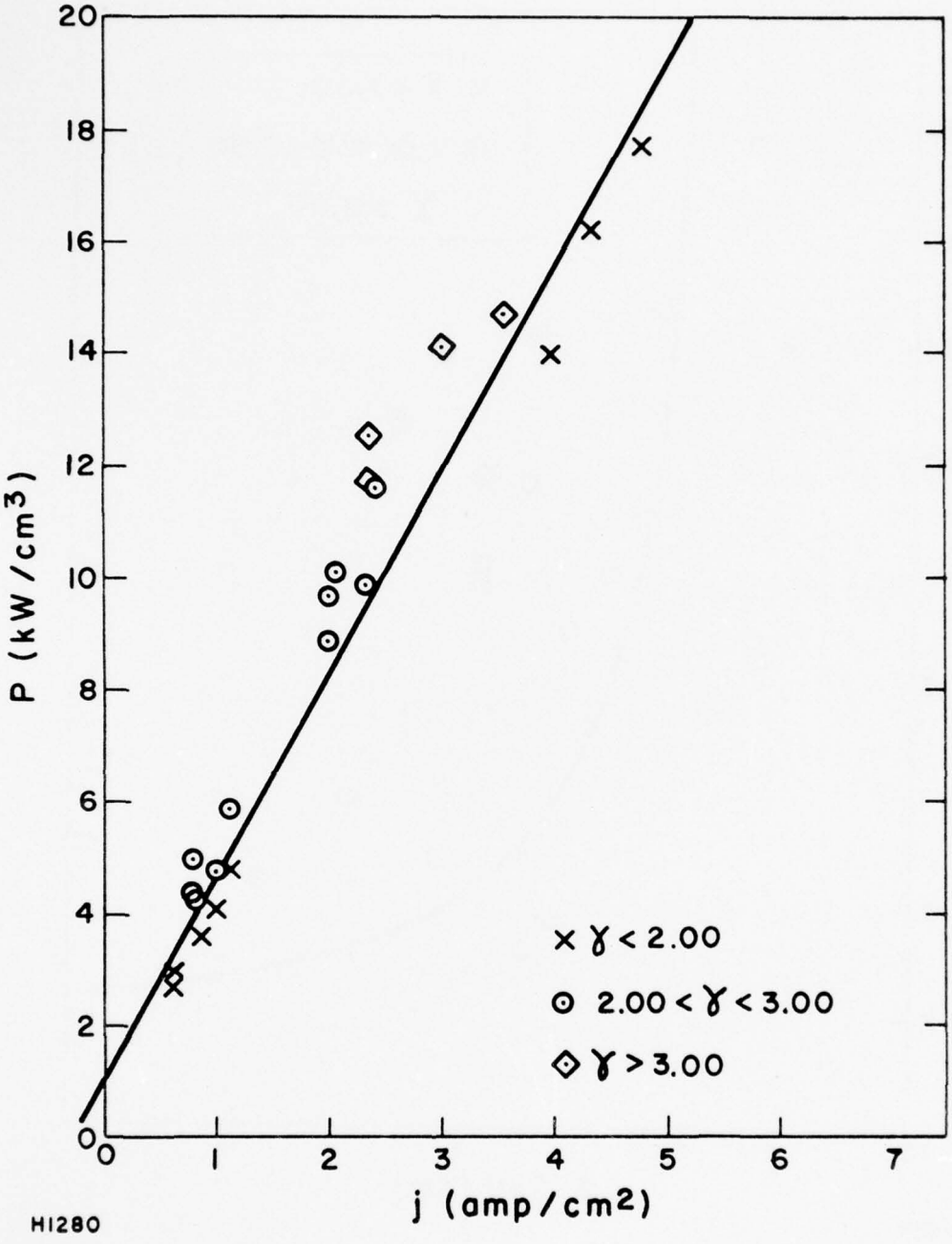

Fig. 16 Dependence of Streamer Growth Rate Upon Discharge Power Density and Current Density. γ is in units of $(100\,\mu\text{sec})^{-1}$.

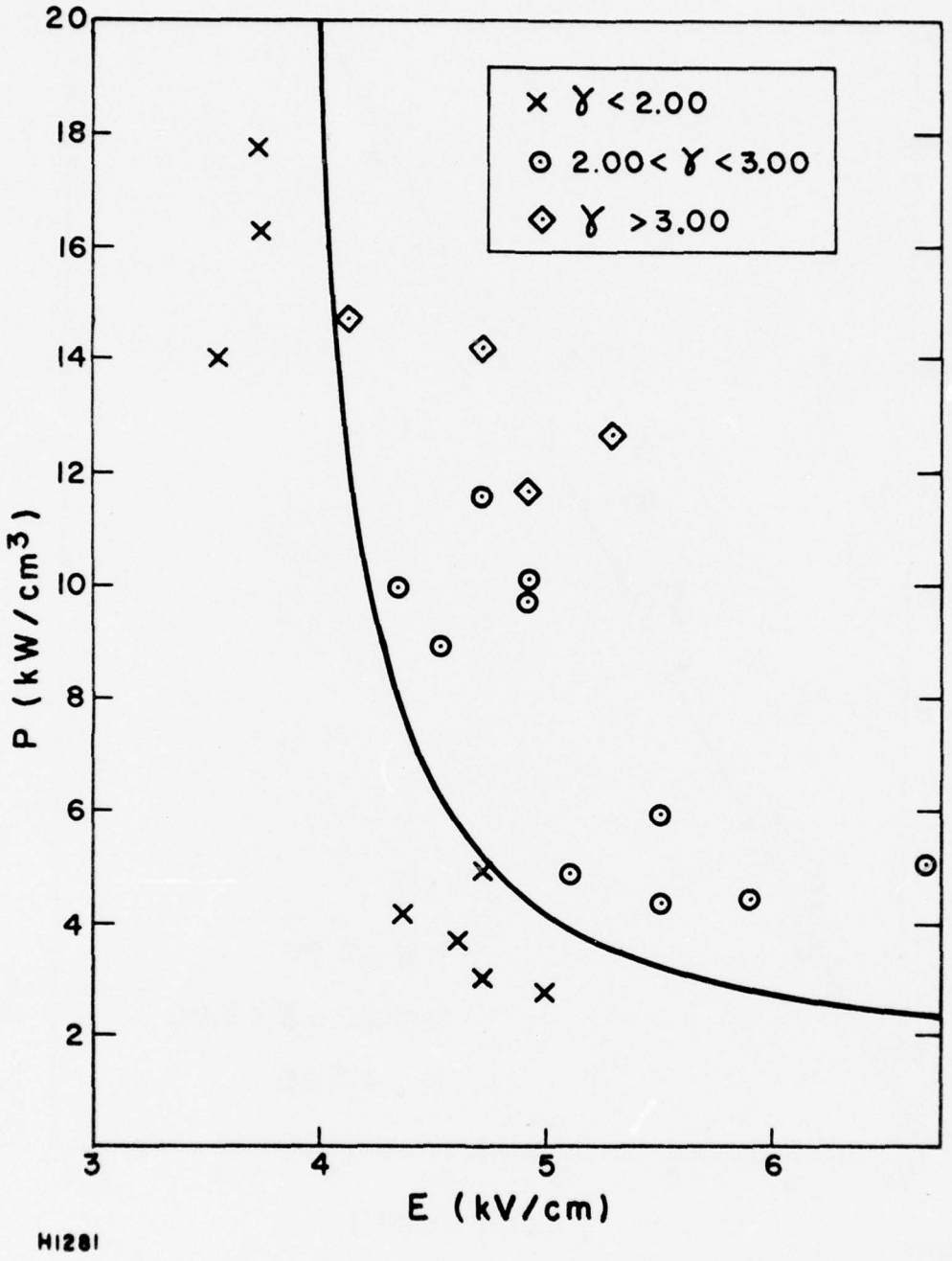

Fig. 17 Dependence of Streamer Growth Rate Upon Discharge Power Density and Electric Field. γ is in units of $(100\ \mu sec)^{-1}$.

the line is a hyperbola. At large powers, the line is nearly vertical, implying that γ is there dependent primarily upon E. But at lower powers and higher electric fields, the line is nearly horizontal, indicating that γ is mainly P dependent in that region.

C. DISCUSSION OF RESULTS

1. Comparison with Theory

Using Eq. (18) we can calculate streamer length versus time for the nitrogen discharge shown in Figs. 12a and 12b, for which E_o = 3000 V/cm, $\sigma_o \simeq 2.7 \times 10^{-4}$, N = 1 and T = 6200°K. The power loading is thus approximately 2.4 kW/cm^3; there is some uncertainty in σ_o since electron density has not been directly measured, due to the electrode geometry. The streamer lengths calculated for various power loadings are shown in Fig. 12b, together with the measured experimental curve. For most of its existence in this discharge the streamer should be moving at sonic velocity. There appears to be farily good agreement between experiment and theory in this case. Considerable data also exists on arcing times in discharges of various dimensions. Since we can approximately identify the arcing time with the streamer transit time across the discharge, a comparison between these results would be interesting. In Fig. 18 the expected transit time for streamers of various lengths in the atmospheric pressure gas mixture He: N_2: CO_2 3:2:1 is shown as function of power loading. Experimental measurements of arcing limits for the discharge device used in the above experiments, with electrode spacing D = 2.54 cm, are shown as crosses and open squares. One experimental arc was obtained in another device with spacing D = 20 cm, which is shown as a solid circle. The experimental scatter may be caused by streamers simultaneously initiating on opposite sides and meeting halfway, thus reducing the arcing time. There is also some uncertainty in the delay time before streamer initiation, which would have the opposite effect.

Experiments have also been performed in a device with D=4 cm which can be operated at 200°K or 300°K. The effect of starting at low temperature

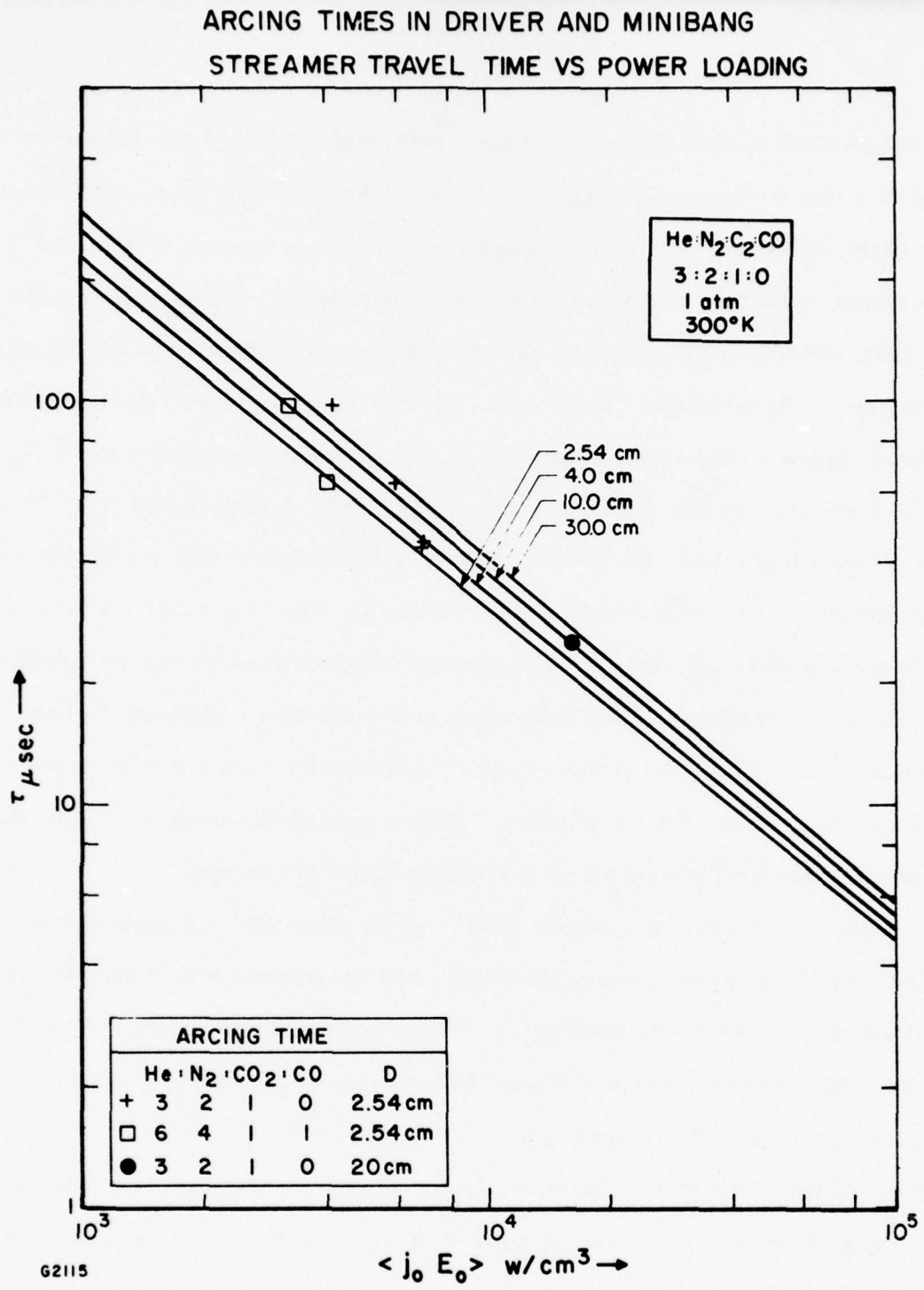

Fig. 18 Streamer Transit Time vs Power Loading in Nitrogen, for Various Electrode Separations (D). Experimental points from cavities with D = 2.54 cm and D = 20 cm are shown.

will be greatest during the sonic propagation regime, since the streamer will move at a lower velocity during this phase. The subsonic phase will change very little, however, since the energy required to go from 200°K to 300°K is a very small fraction of that required to reach 6200°K. In the supersonic phase the streamer will move at 2/3 its previous velocity due to the increased gas density. Experimental results for arcing times together with theoretical streamer transit times are shown in Fig. 19. The gas mixture is 85% N_2, 10% CO_2 and 5% CO, so that its thermal properties are dominated by N_2. The presence of carbon atoms in the heated streamer gas implies that the stable streamer temperature will be near 5350°K (see Section II, Fig. 7), since the ionization potential is lower. Again, the experimental scatter may be due to simultaneous formation of streamers which then meet in the middle. Although the 200°K cases are close to the 4 cm discharge theoretical time, the 300°K cases arc out some 10% sooner than predicted. This is probably caused by longitudinal electron beam shields present at the edges of the discharge.

Since the framing camera studies were done only for pure nitrogen discharges at one atmosphere, that data does not permit a comparison with the predicted pressure dependence or ionization potential scaling. However, we can test the theory against the observed form of the streamers, their temporal growth, and the scaling of growth rate with discharge parameters displayed in Figs. 16 and 17. As already noted, the framing camera photographs do show a streamer structure composed of a luminous column of gas with a ball on the end, as sketched in Fig. 4.

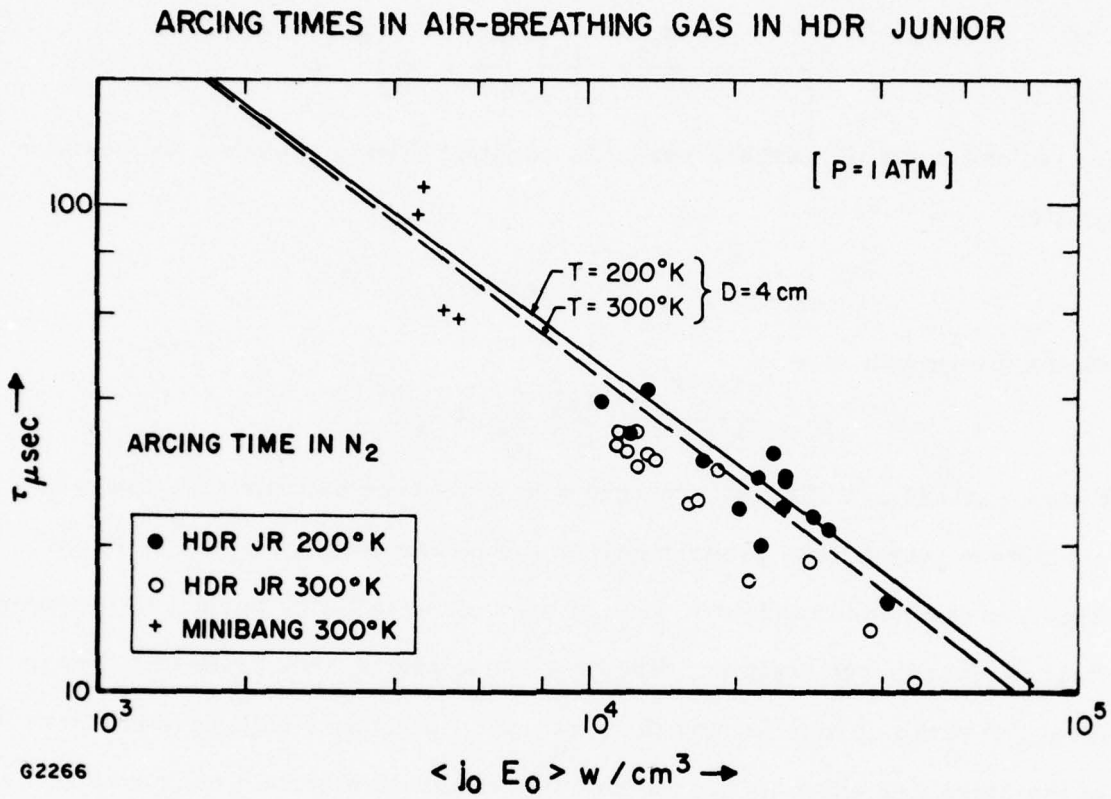

Fig. 19 Streamer Transit Time for Cavities with Various Separations Predicted for 200°K and 300°K N_2 Discharge at 1 atm. Experimental arcing times are shown for 200°K and 300°K in N_2: CO_2: CO 0.84: 0.01: 0.06.

The framing camera data also show the streamers growing exponentially. Such growth is quite consistent with the theory, as can be seen by rewriting Eq. (15) for the subsonic velocity as

$$\frac{dc}{dt} = \frac{3\sigma_o E_o^2}{\lambda k \epsilon N} \left[\frac{a}{c}\right] \left[\frac{7}{4} + \frac{c}{a}\right]^2 c$$

If c/a, the streamer aspect ratio, is constant during growth*, this can be written

$$\frac{dc}{dt} = \gamma c$$

where the growth rate is

$$\gamma = \frac{3\sigma_o E_o^2}{\lambda k \epsilon N} \left[\frac{a}{c}\right] \left[\frac{7}{4} + \frac{c}{a}\right]^2$$

Hence, unless c/a changes strongly with discharge parameters, the theory predicts a growth rate proportional to the power loading, $\sigma_o E_o^2$. From Fig. 17, one sees that this is true at high electric field, but not in the weak-field, high-current regime. Since the assumptions underlying our theory (e.g., that the corona around the streamer tip extends well beyond the radius of the streamer column) are appropriate to the strong field operating mode, one expects agreement with experiment there, as is borne out by our data. In the high current, low field regime, the resistive heating of the gas beyond the streamer tip, i.e., beyond the region of the breakdown field, would have to be considered. Since such heating has not been considered in the present analysis, the lack of agreement there is not surprising.

This conclusion is also supported by the lack of a sonic barrier to streamer propagation under such conditions. Several of the framing camera

---

* From the theory, one expects this to be at least approximately true, an expectation which is borne out by the framing camera photographs.

sequences showed exponential growth continuing unimpeded into a velocity range which would be supersonic for the background gas. Evidently, the streamer was growing into gas already heated by the intensified current ahead of the streamer. Such heating, which turns on smoothly as the streamer approaches, raises the sound speed and hence prevents any abrupt change in behavior as the growth goes supersonic relative to the cold background gas. Again, such behavior is characteristic of the current-dominated regime, which is not of much interest for a laser amplifying medium. In the regime which is of interest, the theory agrees well with our data.

2. Predictions of Arcing Limits for Discharges

Streamer behavior is most concisely described by calculating a maximum loading energy $E_{max} = j_o E_o \tau_A$, where τ_A is the time taken for streamers to cross the discharge. Using the appropriate values from Eq. (18), these loading energies have been calculated for the gas mixture $He:N_2:CO_2$:3:2:1 at atmospheric pressure, and are shown in Fig. 20a as a function of the discharge power loading. The parameter D is the discharge electrode spacing in centimeters. Physically the flat portion of the curve at low power corresponds to the subsonic regime. For wider discharges the sonic and supersonic regimes are reached in the discharge; since the streamer is as it were delayed by the sonic regime more energy can be introduced before the streamer transits and causes arcing. Increasing power input causes the sonic regime to move closer to the initiating electrode. An experimental point corresponding to the only observed arc in a device with D = 20 cm is indicated.

As the pressure is reduced the thermal diffusivity of the gas increases. Consequently the streamer radius b, and the diameter of the cap sphere 2a, will both increase from Eq. (16). This results in relatively slower longitudinal

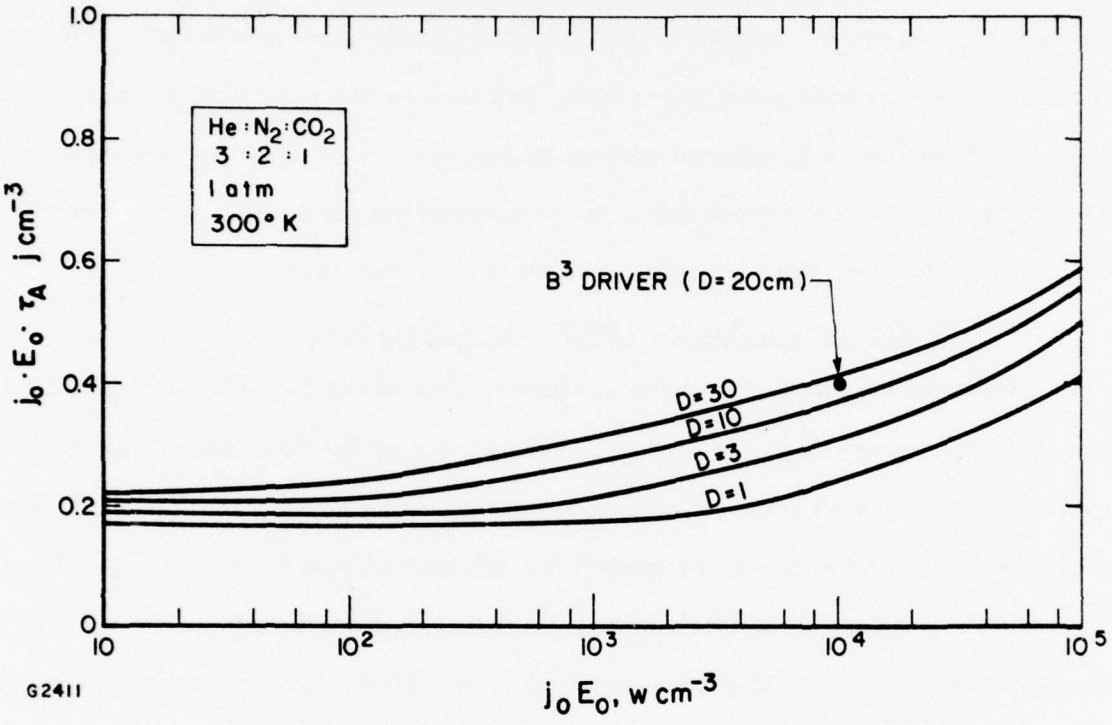

Fig. 20a Loading Energy at Streamer Transit in Discharge at 1 atm

movement of the streamer, since while the current collected increases as the square of the radius, the gas to be heated increases as the cube, causing slower heating. Consequently, at low pressures more energy can be introduced per molecule of gas than at high pressures before the streamer reaches the opposing electrode and arcing ensues. The predictions for the same gas at 1/10 atm are shown in Fig. 20b. We note that it has been known empirically for some time that arcing occurs "later" in EB discharges at low pressure than at high pressure. In the present model this is due only to the dependence of the streamer lateral dimensions on the gas thermal diffusivity.

It is interesting to see that for typical CW discharge conditions we would expect to be almost wholly in the subsonic regime. Consequently the discharge energy loading will be lower than at the high power loading conditions typical of pulsed operation, despite the effect of increased diffusivity mentioned above. This is the reason for the lower specific energy input possible in CW discharges. A point corresponding to HPL-10 (which actually operates in He: N_2: CO_2: CO 6: 4: 1: 1 at 1/10 atm) is indicated in Fig. 20b, which was calculated for 3 : 2 : 1 : 0. Since these two gas mixtures have very similar thermal properties and effective ionization potentials, their behaviour should be close. In fact it appears that HPL-10 arcs at a lower loading than predicted on this model. This could be due to the presence of low ionization potential contaminants in the gas.

3. Effect of Impurities

The effect of a small amount of easily ionized substance on the discharge streamer temperature has been discussed above. We observe from Fig. 7 that 0. 1% molar of sodium decreases the streamer steady state temperature to $T \cong 3500^{\circ}K$, and consequently the streamer can move more

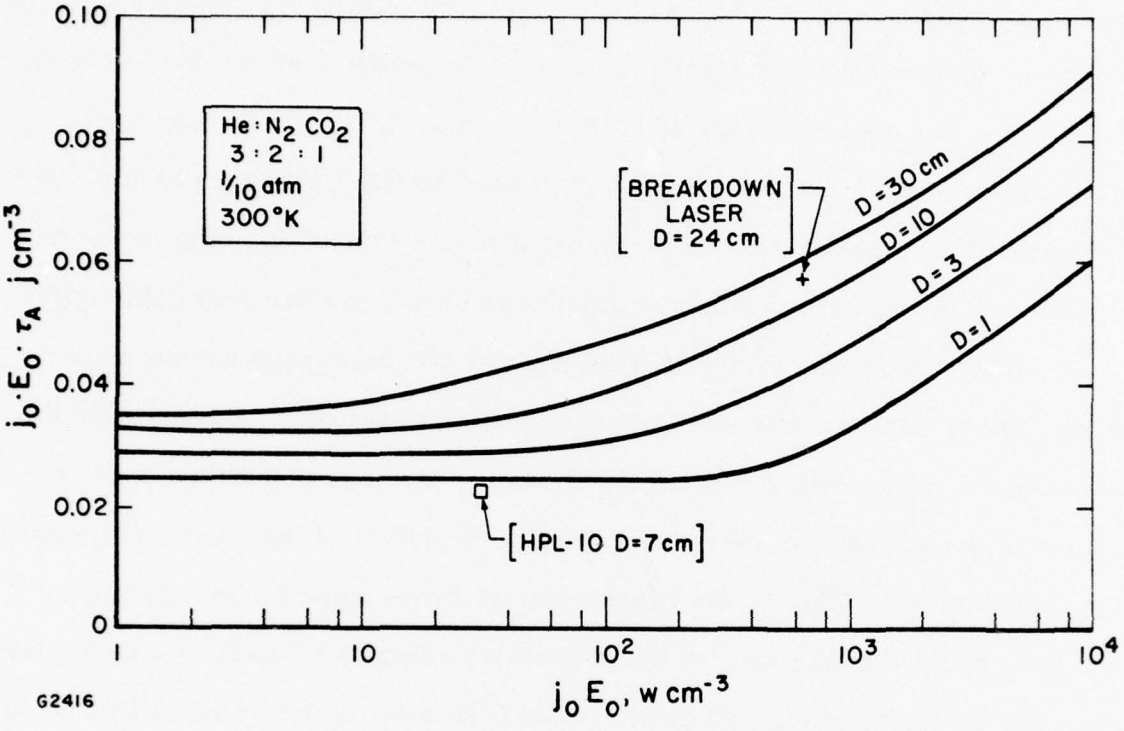

Fig. 20b Loading Energy at Streamer Transit in Discharge at 1/10 atm

rapidly since it heats the gas to a lower temperature: numerically the arcing time is reduced to 70% of its value in pure gas. It is clear that any potassium compounds present will have an even more drastic effect. The presence of easily-ionized material will thus increase the likelihood of arcs, and for discharges operated just below the arcing limit, as is usually the case, we expect even very small amounts of contaminant to initiate arcing. In CW discharges the same effect would be produced by any low ionization potential organic compound present in the gas flow.

D. INITIATION OF STREAMERS

The process of streamer initiation at electrodes usually occurs on a discontinuity or projection. This presumably takes place because the electric field intensification near a projection results in more rapid heating of the gas at that point, and this continues until the gas reaches a temperature at which its conductivity becomes high enough to begin propagating as a streamer, as discussed previously.

There must be a critical size for such a projection to cause a streamer, for if the projection is very small conductive gas cooling will be so rapid that the steady-state temperature reached will be below that required for a stable streamer. Although streamers could ultimately form at such projections, this would be on a time scale corresponding to that required to heat the entire discharge to a conductive temperature, rather than a small part of it.

We will estimate the heating that occurs near a spheriodal protrusion on an electrode.

Considering a spheroidal protrusion of height c and base radius b, we can write the field enhancement near the tip as

$$\beta = \frac{E_{tip}}{E_o} = \left[\left(\eta_o^2 - 1\right)\left\{\frac{1}{2}\ \ell n \frac{\eta_o + 1}{\eta_o - 1} - 1\right\}\right]^{-1} \qquad (20)$$

where $\eta_o = (1 - b^2/c^2)^{-1/2}$, and limiting ourselves to a volume whose radial dimension is the radius of curvature of the spheroidal tip, which is $\rho \approx \frac{b^2}{2c}$, we equate the volumetric conductive cooling from Eq. (1) with the volumetric heating rate, and obtain:

$$\frac{A\, T\, \bar{\kappa}}{\rho^2} = \sigma\, E_o^2\, \beta^2$$

or

$$b = \frac{2}{b/c} \sqrt{\frac{A\,T\,\bar{\kappa}}{\sigma\,\beta^2 E_o^2}}$$

We note that for one-dimensional planar wall-dominated conductive cooling $A \approx 2$; for cooling of a cylinder $A \approx 15$ as before, and we will use the latter value.

The critical base radius for a spheroidal protrusion in a nitrogen discharge at 1 atm is shown in Fig. 21 as function of spheroidal aspect ratio b/c and discharge power loading σE_o^2. The final temperature is taken as $T = 6200^{\circ}K$. For $b/c = 1$ we have a hemispherical boss on the electrode, and for this the maximum field is always three times the discharge field, regardless of radius, so that the heating rate at its tip is always nine times the ambient heating rate. However, if the initial heating takes place in a thin layer, equating layer thicknesses with radius of curvature as above is incorrect. We would then expect the initiation time lag to be much greater than estimated here, and to correspond to the time required to heat up the electrode surface itself—essentially infinite by comparison to the times considered here.

If the protrusion is larger than the critical diameter 2b, then volume heating will take place and the effect of surface heat loss will reduce the volume heating rate only slightly, and may be neglected. We may then estimate the latent time taken to heat the gas in the neighborhood of the protrusion as:

$$\tau_L = \frac{\epsilon\,(T)}{[j \cdot E]} ,$$

where $\epsilon\,(T)$ is the $C_v C_p$ enthalpy (see Appendix A) required to raise unit volume of gas to the temperature T at which the electrical

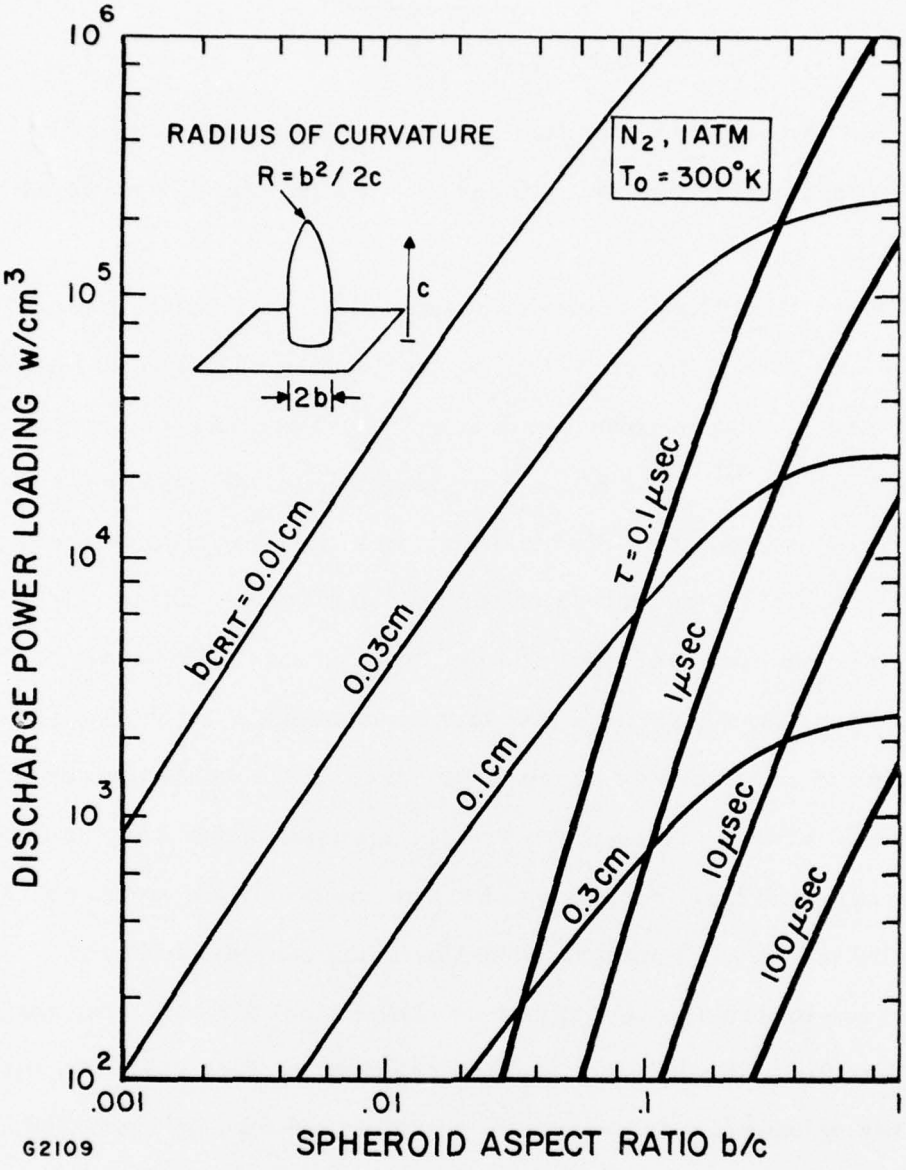

Fig. 21 Streamer Critical Radius and Latent Period for Spheroidal Protrusion

conductivity is high enough for streamer propagation, and $[j \cdot E]$ is the power loading per unit volume of gas near the electrode.

The electrode power loading per unit volume is very much greater than in the main discharge, and especially at the cathode. As pointed out by Cobine,[10] the current density required near the cathode is typically near 15 amp cm^{-2} in the glow discharge at high pressure: the discharge contracts so that electrons actually leave the cathode only over a small fraction of its surface. For a 500 V cathode drop, with cathode layer thickness $\sim 10^{-3}$ cm, the power loading will be 3000 MW/cc. Under these conditions τ_L is negligible and we may assume that streamers form instantly at the cathode and begin their progress across the discharge. At the anode there will be some delay and we anticipate preferential streamer formation on discontinuities; we also expect them to be shorter. Since arcing probably corresponds to cathode streamers completing the discharge transit, we would expect the transit durations discussed previously to be the arcing times, and would predict negligible initiation delay.

E. CONCLUSION

Simple physical assumptions lead to an analytic model for streamers in non-self-sustaining discharges. This model predicts streamer behavior similar to that observed, and discharge arcing times calculated from it are quite close to experimental values, for a variety of pulsed and CW discharges. Framing camera photographs have confirmed the anticipated structure of the streamer. Scaling laws derived for streamers are in accordance with observed results. The effect of low ionization potential contaminants is to reduce streamer temperature and thus result in more rapid streamer transit and arcing. This model will be developed in more detail in the future.

APPENDIX A

GAS SPECIFIC HEATS

A. CONSTANT VOLUME CONSTANT PRESSURE (CVCP) ENTHALPY

In the subsonic regime, the energy required to raise one gram of gas at constant pressure from temperature T_o to T is equal to the enthalpy difference between these temperatures. Writing enthalpy as q(T), the energy is $\Delta Q = q(T) - q(T_o)$ joules per gram. The energy required to raise unit volume of gas over the same temperature range at constant pressure will then be

$$\epsilon = \int_{T}^{T} \rho \left(\frac{\partial q}{\partial T}\right) d T' .$$

where ρ is gas density at temperature T', and $C_p = \frac{\partial q}{\partial T}$. Under these conditions $\rho = \rho_o T_o / T'$, where ρ_o is density at $T = T_o$, and

$$\epsilon = \rho_o T_o \int_{T_o}^{T} \left(\frac{\partial q}{\partial T}\right) \cdot \frac{dT'}{T'} . \qquad \text{(A-1)}$$

Fortunately ϵ can generally be represented fairly well by a simple power law for most molecular gases. We note that in the case of a perfect monatomic gas we can immediately write

$$\epsilon = 5/2 \, N_o \, kT_o \, \ell n \, (T/T_o),$$

where N_o is initial number density at $T = T_o$ and k is Boltzmann's constant. In the case of molecular gases the energy used in exciting different vibrational modes, rotation, and dissociation must be included,

as well as the fact that the gas density under constant pressure will decrease more rapidly than 1/T.

1. Helium

Treating this as a perfect monatomic gas and ignoring ionization for $T < 15,000^{\circ}K$, we take initial conditions as $T_o = 300^{\circ}K$ and P = 1 atm:

$$\epsilon_{He} = 0.254 \ln (T/T_o) \text{ J/cm}^3 . \qquad \text{(A-2)}$$

2. Nitrogen

Using the thermodynamic tables[6] for N_2, Eq. (A-1) is plotted in Fig. A-1. A suitable fit for the region of interest is

$$\epsilon_N = \epsilon_o (T/T_1)^{\alpha}, \qquad \text{(A-3)}$$

with $\epsilon_o = 1$ J/cc and $T_1 = 3500^{\circ}K$, $\alpha = 0.63$.

3. Carbon Dioxide

The constant pressure enthalpy for CO_2 is shown[11] in Fig. A-2 The best fit for the energy required to heat 1 cm^3 to temperature T is then:

$$\epsilon_{CO_2} = (T/T_3)^{\mu} \text{ J cm}^{-3} \qquad \text{(A-4)}$$

where $T_3 = 691^{\circ}K$ and $\mu = 0.71$.

B. NUMERICAL STREAMER ENERGIES IN THE SUBSONIC REGIME

Using the above values of the constant-volume constant-pressure ($C_v C_p$) enthalpy for the gas mixtures $He:N_2:CO_2:CO$ 0:1:0:0, 3:2:1:0, 0:3:1:0, 16:8:1:0, we obtain the following limiting energies at which streamers can exist in these gases at atmospheric pressure.

1. Nitrogen

$$\epsilon(T) = (T/3500)^{0.63}, \quad N = 1, \quad T = 6200^{\circ}K .$$

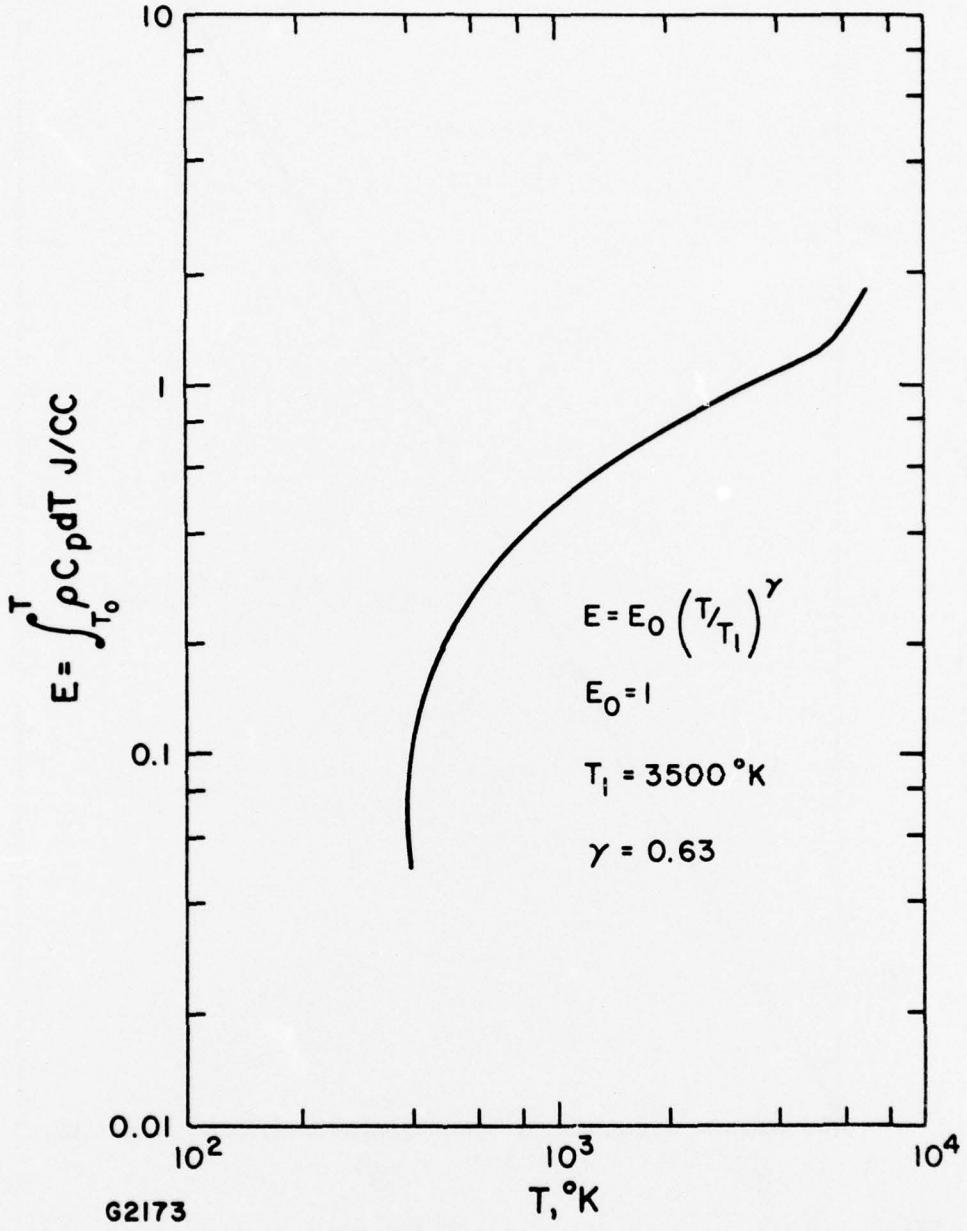

Fig. A-1 CVCP Enthalpy of Nitrogen

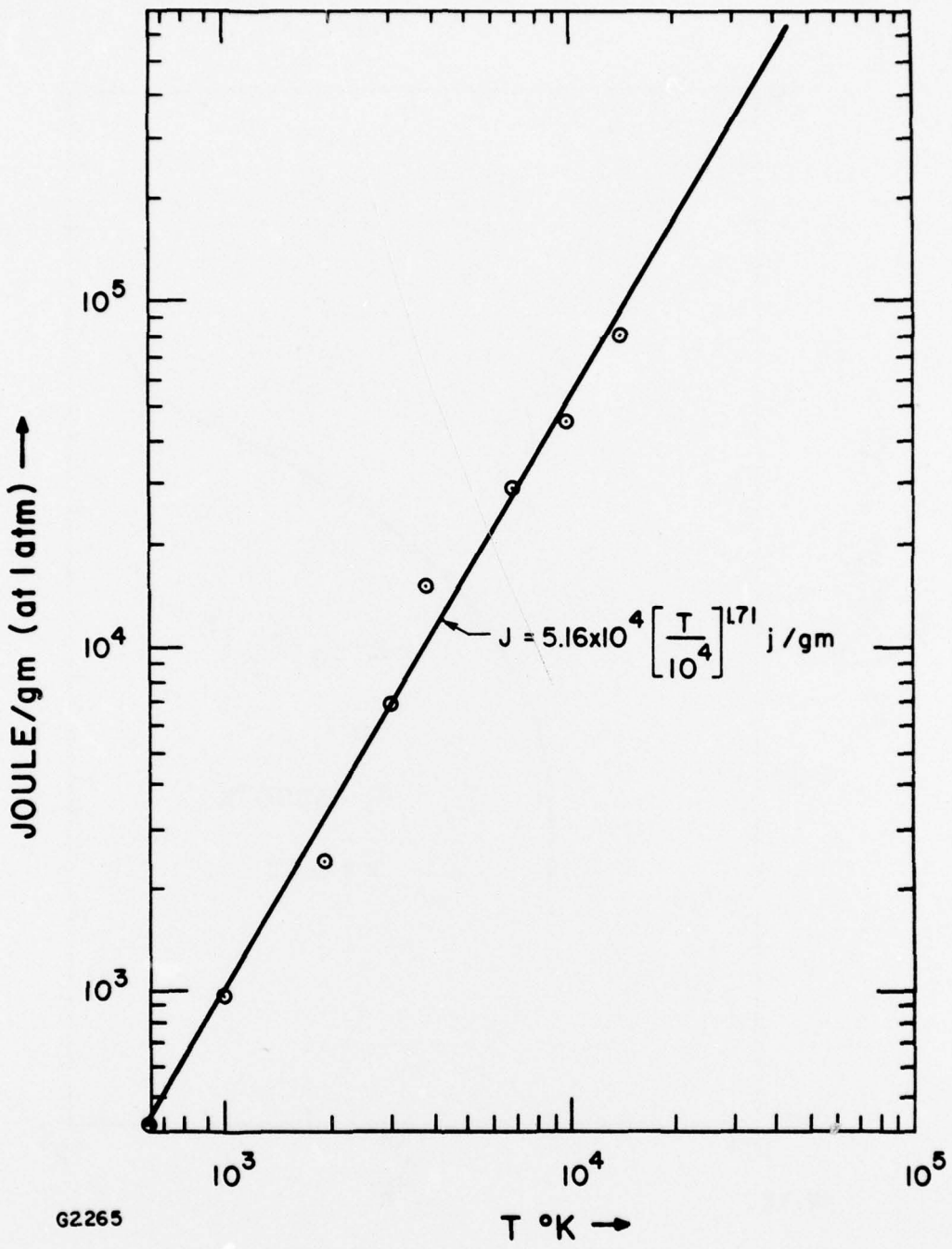

Fig. A-2 Constant Pressure Enthalpy for CO_2

Hence

$$\epsilon = 1.43 \text{ J/cm}^3$$

2. $\underline{He:N_2:CO_2:3:2:1}$

The most readily ionized component of this mixture when dissociated will be the 10% carbon atoms, and using this in the Saha equation and solving (5) gives the line shown in Fig. 7, from which we obtain $T \sim 5350^{\circ}K$ for streamer formation under typical conditions. Using the CVCP enthalpy for each component, we get

$$\epsilon \approx 1/6 \left[3 \times 0.254 \ell n (T/300) + 2 (T/3500)^{0.63} + (T/691)^{0.71}\right],$$

or

$$\epsilon \approx 1.51 \text{ J/cc at } 5350^{\circ}K.$$

3. $\underline{He:N_2:CO_2:CO\ 3:2:\frac{1}{2}:\frac{1}{2}}$

This gas may be expected to have virtually the same thermal behavior as 3:2:1:0 at 1 atm.

4. $\underline{N_2:CO_2:H_2\ 3:1:0.08}$

We may apply the above reasoning and obtain a molar fraction 11% carbon atoms in the dissociated gas, giving essentially the same critical temperature $T \sim 5350^{\circ}K$. The CVCP enthalpy is then

$$\epsilon \approx \frac{1}{4} \left[3 \times (T/3500)^{0.63} + (T/691)^{0.71}\right].$$

or

$$\epsilon \approx 2.05 \text{ J/cc at } 5350^{\circ}K.$$

5. $\underline{He:N_2:CO_2:16:8:1}$

The critical temperature in this gas will be near $6000^{\circ}K$ due to its lower carbon content. Using Appendix A gives the corresponding CVCP enthalpy as $\epsilon \approx 1.12$ J/cc at $6000^{\circ}K$.

C. INTERNAL ENERGY

In the supersonic regime expansion of the gas during the heating process may be neglected, and the total energy required is the difference in internal energy between the lower and higher temperatures. Again, for a monatomic gas with negligible ionization this will be:

$$\epsilon = \frac{3}{2} R \Delta T$$

while for molecular gases the contributions from dissociation and ionization must be included.

1. Helium

$$\epsilon = \frac{3}{2} N_o k \Delta T \text{ J cm}^{-3}$$

2. Nitrogen

In the thermal regime 5000-6000°K, for gas, initially at atmospheric pressure and 300°K, we have:

$$\epsilon \approx 10.6 \left[\frac{T}{5000}\right] \text{J cm}^{-3}.$$

Thus at 6200°K, ϵ = 13.1 J cm^{-3} and 5350°K, ϵ = 11.3.

3. Carbon Dioxide

In the thermal regime 5000-6000°K, for gas initially at atmospheric pressure and 300°K, we have:

$$\epsilon \approx 13.68 \left[\frac{T}{6200}\right] \text{J cm}^{-3}.$$

Thus at 5200°K, ϵ = 13.68 J cm^{-3} and at 5350°K, ϵ = 11.8.

4. $He:N_2:CO_2$ 3:2:1

For this mixture initially at atmospheric pressure and 300°K, the weighted average of the above quantities yields:

$$\epsilon = 1.33 \times 10^{-3} T \text{ J cm}^{-3}, \text{ where } 5000 < T \leq 6000.$$

Thus for T > 5350°K, ϵ = 7.1.

REFERENCES

1. Jacob, J., Avco Everett Research Laboratory, Private communication (1972).

2. Rogoff, G., Phys. Flu. 15, 1931 (1972).

3. Raizer, Y.P., Sov. Phys. JETP, 31, 1148 (1970).

4. Zeldovich, Y.B. and Raizer, Y.P., Physics of Shock Waves and High Temperature Hydrodynamic Phenomena, A.P. New York (1966).

5. NACA TN 4150 (1958).

6. Tables of Thermodynamic Properties of Nitrogen from 1500 to 15000°K. Lewis, C.H., Burgess, E.G., T.N. AEDC-TDR-63-138 (1963).

7. Douglas-Hamilton, D.H., J. Chem. Phys. 58, 4820 (1973).

8. Douglas-Hamilton, D.H. and Mani, S.A., J. App. Phys. 45, 4406 (1974).

9. Kivel, B., AERL Research Report 79, "Radiation from Hot Air and Stagnation Heating," October 1959.

10. Cobine, J.D., Gaseous Conductors, Dover (1958).

11. Table of Thermodynamics Properties of Carbon Dioxide, Bailey, H.E., NASA SP-3014 (1965).

SECURITY CLASSIFICATION OF THIS PAGE (When Data Entered)

REPORT DOCUMENTATION PAGE

READ INSTRUCTIONS BEFORE COMPLETING FORM

1. REPORT NUMBER: AFOSR-TR-78-0354	2. GOVT ACCESSION NO.
3. RECIPIENT'S CATALOG NUMBER	
4. TITLE (and Subtitle): ELECTRON-BEAM SUSTAINER DISCHARGE STREAMERS AND ARCING,	5. TYPE OF REPORT & PERIOD COVERED: FINAL rept. 1 Dec 74 - 30 Nov 77
	6. PERFORMING ORG. REPORT NUMBER
7. AUTHOR(s): D H DOUGLAS-HAMILTON, P S ROSTLER	8. CONTRACT OR GRANT NUMBER(s): F44620-75-C-0025
9. PERFORMING ORGANIZATION NAME AND ADDRESS: AVCO EVERETT RESEARCH LABORATORY, INC, 2385 REVERE BEACH PARKWAY, EVERETT, MA 02149	10. PROGRAM ELEMENT, PROJECT, TASK AREA & WORK UNIT NUMBERS: 2308C1, 61102F
11. CONTROLLING OFFICE NAME AND ADDRESS: AIR FORCE OFFICE SCIENTIFIC RESEARCH/NA, BLDG 410, BOLLING AIR FORCE BASE, D C 20332	12. REPORT DATE: Nov 77
	13. NUMBER OF PAGES: 78 (79 p.)
14. MONITORING AGENCY NAME & ADDRESS (if different from Controlling Office)	15. SECURITY CLASS. (of this report): UNCLASSIFIED
	15a. DECLASSIFICATION/DOWNGRADING SCHEDULE

16. DISTRIBUTION STATEMENT (of this Report)

Approved for public release; distribution unlimited.

17. DISTRIBUTION STATEMENT (of the abstract entered in Block 20, if different from Report)

18. SUPPLEMENTARY NOTES

19. KEY WORDS (Continue on reverse side if necessary and identify by block number)

ELECTRON BEAM DISCHARGE
STREAMERS
DISCHARGE STABILITY
LASER

20. ABSTRACT (Continue on reverse side if necessary and identify by block number)

The electron beam sustainer method of generating a stable high pressure gas discharge is investigated theoretically and experimentally. The most important discharge instability in the non-self-sustaining discharge is the steamer; this is discussed and a model proposed for formation and propagation. Integration of streamer velocity over the discharge gap predicts arcing times. Experimental measurements of streamer behavior in nitrogen discharge have been made, and these are compared with predictions. Comparisons in other gas mixtures and various electron-beam sustainer discharge devices have also been made.

DD FORM 1 JAN 73 1473 EDITION OF 1 NOV 65 IS OBSOLETE

048 450

UNCLASSIFIED

SECURITY CLASSIFICATION OF THIS PAGE (When Data Entered)